Prochlorococcus Growth Responses to Light and Oxygen Regimes

By

Laurel Genge

A thesis submitted to the
Department of Biology
Mount Allison University
in partial fulfillment of the requirements for the
Bachelor of Science degree with Honours
April 16th, 2021

Table of Contents

Acknowledgements

I thank my thesis supervisor, Dr. Douglas A.Campbell, for his guidance and expertise throughout this project. I thank Dr. Andrea Morash, my committee member, along with Maxmillian Berthold who helped me with Multi-Cultivator set-up and technological glitches. I would also like to thank Mireille Savoie for helping me with cell harvesting protocols and Carlie Barnhill for assisting with Multi-Cultivator runs and writing RStudio script.

Abstract

Prochlorococcus is a genus of very small marine picocyanobacteria characterized by an unusual green pigmentation, because they lack the phycobilisomes characteristic of most cyanobacteria. *Prochlorococcus* belongs to the phylogenetically diverse functional group of photosynthetic picophytoplankton and is the most abundant photosynthetic organism on earth. In aquatic environments, phytoplankton, and specifically *Prochlorococcus*, metabolism represents a major source of extracellular reactive oxygen species (ROS). If left un-scavenged ROS can have detrimental effects on marine phytoplankton growth and survival. Different *Prochlorococcus* strains grow stratified in marine aquatic environments from the surface to the bottom of the illuminated euphotic zone. Strains of *Prochlorococcus* at different depths exhibit diverse responses to light, however, they are slow growing and difficult to culture, with limited analyses of their growth responses. During this project I monitored growth trajectories of diverse *Prochlorococcus* strains across a matrix of light levels, light colors and oxygen levels. I found that each strain shows a distinct pattern of growth rates across the environmental matrices, with *Prochlorococcus* MED4 thriving under a high light, fully oxygenated niche; *Prochlorococcus* SS120 preferring a low light, oxygenated niche and *Prochlorococcus* MIT9313 preferring a low oxygen, high light niche. The combination of blue light and oxygenation is particularly stressful to Prochlorococcus MIT9313. We hypothesize that the oxygen intolerance of *Prochlorococcus* MIT9313 relates to strong sensitivity to ROS. Therefore, we took samples for subsequent analyses of cross linking of the major RbcL protein, a proxy for cumulative effects of ROS exposure. The results presented in this project can be applied to climate change research because it highlights the environmental responses of the foundational organism in marine food webs and bottom-up factors in ecosystem change within marine environments.

Introduction

Overview of Phytoplankton

Phytoplankton are photosynthetic algae that serve as foundations of marine ecosystems. These microscopic organisms mediate marine productivity, elemental cycling, and atmospheric composition, making them vital to marine food webs and stabilizing environmental change (Moore et al., 1995). Major groups of phytoplankton include the taxa of cyanobacteria, green algae, diatoms, and dinoflagellates. The varying shapes and sizes of the phytoplankton species generate ecological diversity and scientific curiosity, in part because size and shape influence diffusional interactions of cells with solutes, including reactive oxygen species (ROS).

Growth rate studies uncover the influences of light and temperature on phytoplankton growth and cumulative physiology (Moore et al., 1995; Perry et al., 1981; Strzepek et al., 2019). Significant research conducted on marine phytoplankton has focused on the picocyanobacteria species *Prochlorococcus* and *Synechococcus* that dominate primary production in many tropical and sub-tropical marine ecosystems (Scanlan et al., 2009). Individual picocyanobacteria strains show distinct growth responses to varying light and nutrient regimes sparking genetic evolutionary questions. In this study the growth responses of three strains of marine *Prochlorococcus* SS120, MED4, and MIT9313 were measured under varying light level, spectral band, and oxygen regimes.

Marine *Prochlorococcus*

Cyanobacteria are photosynthetic organisms that were among the pioneer microorganisms to inhabit Earth between approximately 3.4-2.4 billion years ago (Mazard et al., 2016, Latifi et al., 2009). These prokaryotic cells contributed to the Earth's atmospheric transition from high carbon-dioxide to the oxygen rich environment that we know today, as a result of their oxygenic photosynthesis (Mazard et al., 2016, Falkowski, 1994). Over time, cyanobacteria evolved into a variety of species with diverse morphologies and niches ranging from terrestrial to aquatic environments (Braakman et al., 2017, Irigoien et al., 2004, Scanlan et al., 2009).

Prochlorococcus marinus is a taxa of picocyanobacteria; photosynthetic marine prokaryotes smaller than 1µm in diameter (Partensky et al., 1999). *Prochlorococcus* typically goes through cellular division synchronized with the diel cycle in the subsurface layers of the ocean and dominates oceanic photosynthetic biomass in many tropical and subtropical regions. Phylogenetically, *Prochlorococcus* strains are closely related, with less than 3% difference among their 16S rRNA sequences (Rocap et al., 2003).

Marine *Prochlorococcus* have small genomes ranging from 1.64-2.7 Mb (Scanlan et al., 2009). Researchers have suggested that *Prochlorococcus* strains have decreased their genome size throughout evolution to optimize their nutrient quotas to support their dominance in oligotrophic waters (Rocap et al., 2003). These picocyanobacteria possess a light-harvesting complex that contains divinyl chlorophylls *a* and *b* to capture visible light (Partensky et al., 1999; Rocap et al., 2003). Divinyl chlorophyll *a* exhibits maximum absorption at 442, 620, and 666 nm, while divinyl chlorophyll *b* absorption peaks at 478, 610, and 658 nm (Rocap et al., 2003). The presence of these chlorophyll derivatives allows for *Prochlorococcus* strains to populate deeper portions of the euphotic zone (Partensky et al., 1999). The organisms under investigation here include two strains assigned to low-light ecotypes *Prochlorococcus* MIT9313 and *Prochlorococcus* SS120, and one strain assigned to high-light ecotype *Prochlorococcus* MED4. Overall, *Prochlorococcus marinus* are foundational microorganisms whose growth and metabolism support marine food webs and play a large role in aquatic biological response mechanisms.

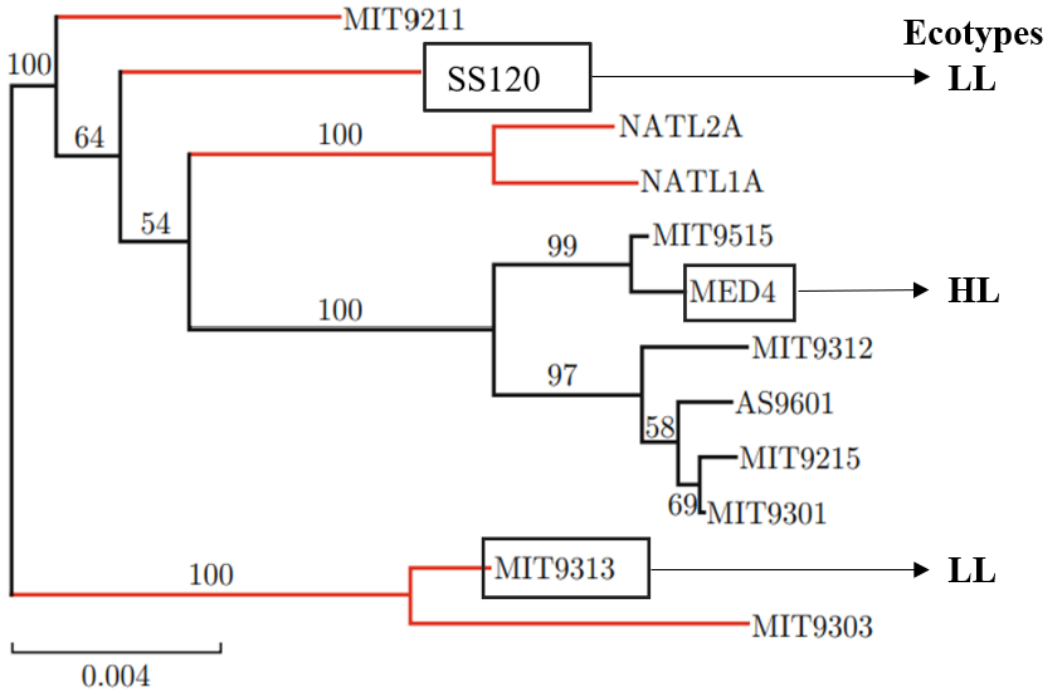

Figure 1. Phylogenetic tree of *Prochlorococcus* strains obtained by alignment of 16S rRNA gene sequences of 12 genomes. Black boxes indicate the strains of *Prochlorococcus* used in this study. Both SS120 and MIT9313 strains are termed low-light (LL) ecotypes represented by red bars, while the MED4 strain is termed a high-light ecotype (HL) represented by black bars. Image retrieved from Prabha et al., 2014.

Ocean Niche Partitioning

The dominance of *Prochlorococcus marinus* in warm oligotrophic ocean waters is partially influenced by the genomic diversity of the cyanobacterial genus (Prabha et al., 2014). The genus *Prochlorococcus* includes specific cell types which are identified by their geographic ranges, so far thought to be controlled by temperature, spectral ranges, and nutrient regimes (Six et al., 2007). Although *Prochlorococcus* strains can coexist within a water column, across ocean basins their distribution is structured by a combination of environmental variables, notably irradiance (Larkin et al., 2016). Hence, the major phylogenetic clades of *Prochlorococcus* are often referred to as 'ecotypes' due to their niche partitioning based on nutrient and light regimes (Johnson et al., 2006; Thompson et al., 2013).

Although diverse *Prochlorococcus marinus* ecotypes are found vertically stratified in the same water column the average irradiance has a strong contribution to depth niche partitioning (Moore and Chisholm, 1999). As the ocean water column mixes the phytoplankton cells can move vertically through a large gradient of depth and irradiance. The downward mixing of phytoplankton cells causes a decrease in light irradiance, up to 200m deep where the light level drops as low as 0.1% of surface radiance (Moore and Chisholm, 1999). In contrast, when a cell is taken upwards in the water column it must withstand a rapid and large increase in irradiance (Six et al., 2007). Due to fluctuations in irradiance depending on water column depth *Prochlorococcus* populations exhibit large changes in the ratio of Chl *b* to divinyl Chl *a* and flow cytometrically derived chlorophyll fluorescence per cell with depth. In addition to cytofluorometry, non-parametric local regression models have been used to predict the global *Prochlorococcus* cell abundance based on temperature and photosynthetically active radiance (PAR) (Flombaum et al., 2013; Moore and Chisholm, 1999). Collectively, these metrics suggest that there are two major ecotypes of *Prochlorococcus* coexisting in the oceans: one acclimated to the low light and high nutrient conditions of the deep euphoric zone and the other acclimated to high light and low nutrient conditions at the surface (Moore et al., 1995; Moore and Chisholm, 1999; Partensky et al., 1999). The species in this study include one high-light ecotype *Prochlorococcus* MED4, and two low-light ecotypes *Prochlorococcus* SS120 (CCMP1375), and *Prochlorococcus* MIT9131 which we grew under a matrix of varying light intensity, colour, and oxygen concentrations to determine growth and physiological responses of each strain under varying environmental regimes.

Climate Change and Predicted Community Structure Change

As atmospheric CO_2 levels continue to increase the threat to the stability of marine ecosystems is becoming more serious through increased ocean temperatures (Cooper et al., 1987) and shifts in biogeochemical cycles. Marine phytoplankton are fundamental organisms in marine food webs contributing approximately half of the net global primary production and play a critical role in regulating global biogeochemical cycles (Flombaum et al., 2013). As mentioned above marine phytoplankton comprise diverse organisms with differences in phylogeny, metabolism and ecological niches. This diversity further shows the importance of understanding the contribution of different phytoplankton groups to ecosystem functionality as a central proxy for predicting the biogeochemical impact of future environmental changes.

Niche-based models have been widely used to predict the response of plant species to future climate change. Similarly these models have been used to represent the realized niche of *Prochlorococcus* species based on the use of resources as the net outcome of bottom-up and top-down processes (Flombaum et al., 2013).

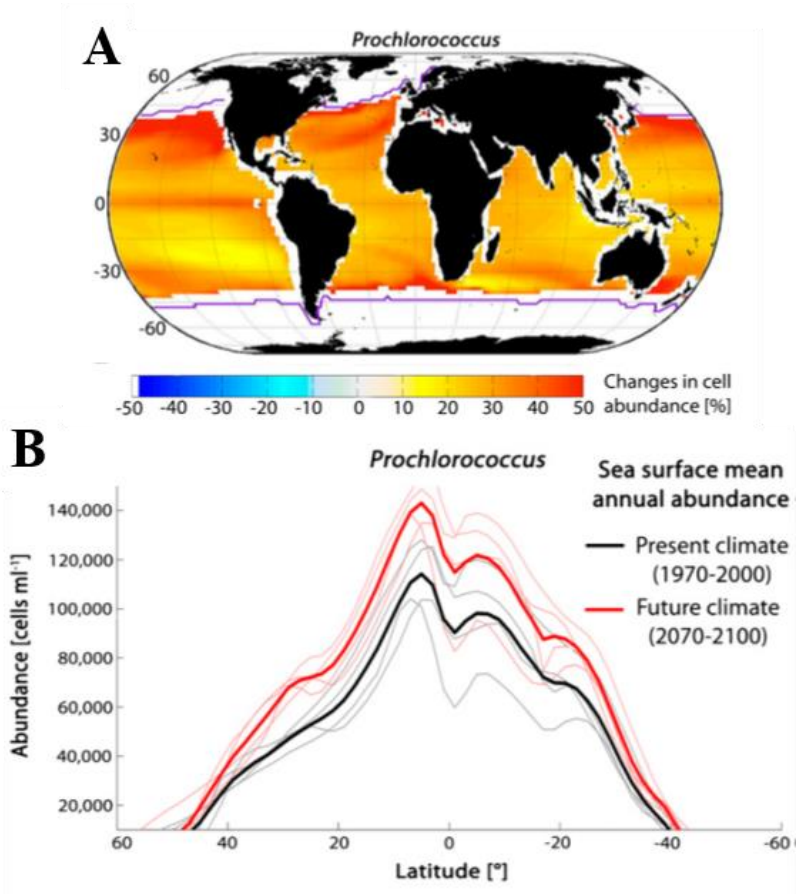

Figure 2. Projected change in global abundance and distribution of *Prochlorococcus* for the year 2100 adapted from (Flombaum et al., 2013).
(A) Percent change in mean annual abundance between present and future climate (end of 20th and 21st century) at the ocean surface. The coloured areas on the map represent the change in abundance in regions with $>10^4$ cells mL^{-1} at present climate. The purple lines represent the distribution limit of 10^4 cells mL^{-1} under future climate.
(B) Mean annual abundance estimated for present and future climate for a north-south transect at the Atlantic Ocean 330° meridian of *Prochlorococcus.* Thick line represents the annual mean for the multimodal ensemble and thin lines for each of the four models.

In Figure 2 a niche-based model shows the estimated sea surface abundances and distributions for *Prochlorococcus* at the end of the 20th and 21st centuries using climate model projections of sea surface temperatures. This multimodel figure projected an average 28.7% increase in *Prochlorococcus* with substantial regional variation in cell abundance (Flombaum et al., 2013). These models provide quantitative evidence for predicting and understanding future populations of *Prochlorococcus* and how these shifts may contribute to large scale changes in phytoplankton communities. Furthermore, due to the significant abundance of *Prochlorococcus marinus* in marine ecosystems these fluxes in population can have noticeable impacts on the fundamental processes of ocean ecosystems and global biogeochemical cycling.

Reactive Oxygen Species and Scavenging

In addition to being a valuable source of oxygen production, *Prochlorococcus marinus* also produce multiple ROS as by-products of their photosynthetic metabolism (Diaz and Plummer, 2018). ROS include intermediates in the four-electron reduction of oxygen to water: superoxide (O_2^-), hydrogen peroxide (H_2O_2), hydroxyl radical (•OH). In parallel the excited state singlet oxygen ($^1O_2$) (Braakman et al., 2017) is produced via excitation energy input into oxygen creating a highly reactive compound with a short half- life that can directly damage target molecules including; lipids, proteins, and pigments. Both O_2^- and •OH have unpaired electrons rendering them highly reactive with biomolecules (Latifi et al., 2009).

H_2O_2 is a key intermediate in many redox reactions and in the photochemical oxidation of dissolved organic matter (Price et al., 1992). H_2O_2 has the potential to harm biomolecules in picocyanobacteria. H_2O_2 is present at relatively high concentration in oligotrophic marine waters and has a relatively long lifetime before decay, compared to other ROS (Table 1). H_2O_2 has the potential to oxidize dissolved organic matter and affects the redox state of trace metals making it an important reactant in the cycling of foundational elements (Kieber et al., 2003).

Table 1. Typical concentrations and lifetimes of reactive oxygen species arranged by lifetime (Diaz & Plummer, 2018, Kieber et al., 2003, Dahl et al., 1987)

Reactive oxygen species		Concentration range in ocean water (mol L^{-1})	Lifetime
Hydrogen Peroxide	H_2O_2	$1x10^{-9}$-$x10^{-6}$	hours-days
Superoxide	O_2^-	$1x10^{-12}$-10^{-9}	seconds-minutes
Singlet Oxygen	$^1O_2$	$1x10^{-15}$-10^{-12}	53±37 µseconds
Hydroxyl Radical	•OH	$1x10^{-18}$-$x10^{-15}$	µseconds

Prochlorococcus marinus produce intracellular ROS in the cytoplasmic and thylakoid membranes via respiration and photosynthesis. In PSII, $^1O_2$ is produced by energy input to oxygen from photosensitized chlorophyll. In PSI, O_2^- is generated by the reduction of oxygen using electrons from PSII. Two molecules of O_2^- are then transformed into H_2O_2 and oxygen gas by superoxide dismutase in the stroma. H_2O_2 is also found extracellularly in the surrounding environment of marine cyanobacteria. Natural causes such as rainfall on the open ocean can increase H_2O_2 concentrations to greater than 10x the baseline concentration of surface water (Cooper et al., 1987). H_2O_2 is sufficiently long-lived to diffuse across cellular membranes, meaning both extra- and intra-cellularly produced ROS contribute to the ocean pool (Diaz and Plummer, 2018). The highly reactive •OH is produced by the reduction of H_2O_2 through the photo-Fenton reaction in the lumen (Latifi et al., 2009). Some mechanisms of intracellular production of ROS in cyanobacteria are visualized in Figure 3.

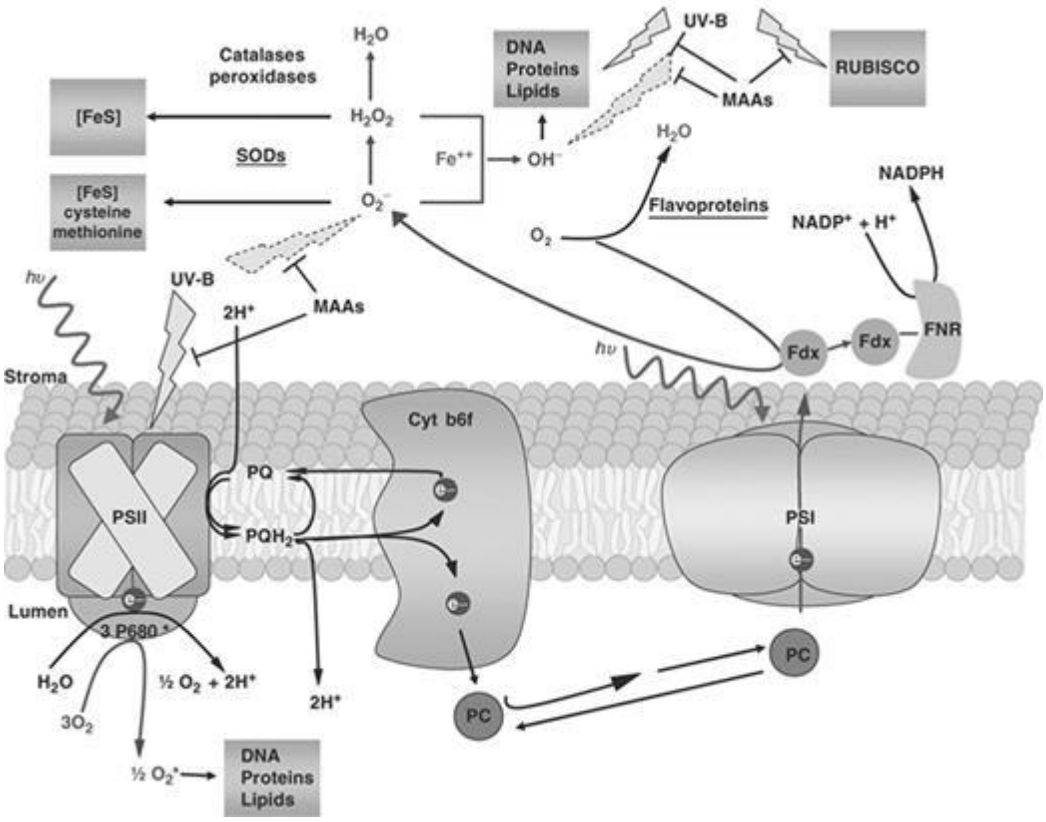

Figure 3. Some known reactive oxygen species production sites and targets within cyanobacteria (Latifi et al., 2009).

Due to the highly reactive properties of ROS they have potentially detrimental effects on cell DNA, proteins and lipids, including the inactivation of photosystems causing photoinhibition in cyanobacterial cells (Latifi et al., 2009). In addition to the damaging effects on biomolecules, ROS help poise the chemical redox state of aquatic systems and have variable biological impacts on other aquatic organisms and ecosystem structure. However, the physiological roles of extracellular ROS released by phytoplankton, and the wider significance to ecosystem-scale trophic interactions and biogeochemistry remain unclear.

Despite previous research on the negative effect of ROS a recent review suggested that biological ROS production may actually promote growth and survival in some phytoplankton species (Diaz and Plummer, 2018). This phenomenon poses interesting physiological questions about marine cyanobacteria and the reason behind their seemingly deleterious production of ROS. The objective of this project is to monitor the growth of different strains of phytoplankton grown at various environmental conditions, leading to analyses to quantify the effects of ROS on the growth of *Prochlorococcus marinus* strains.

RbcL

The *rbcL* gene encodes for the large subunit protein (RbcL) of the Ribulose -1,5-bisphosphate carboxylase/oxygenase (RuBisCO) enzyme (Fernández-Pinos et al., 2015). RuBisCO is one of the most abundant enzymes on the planet allowing photosynthetic organisms to sequester inorganic CO_2 into organic carbon for photosynthesis via the Calvin cycle (Andersson and Backlund, 2008). This enzyme catalyzes the primary photosynthetic CO_2 assimilation reaction where CO_2 is bonded to the 5-carbon acceptor molecule ribulose -1,5-bisphosphate (RuBP) releasing two molecules of 3-phosphoglycerate.

Due to the abundance and multi-subunit stoichiometry of the RuBisCO enzyme the RbcL protein can be used as an indicator of oxidative stress in *Prochlorococcus marinus* cells. In the euphotic zone of marine waters where the cyanobacterium thrives, ROS are continuously produced making these cells highly susceptible to oxidative stress by ROS, specifically H_2O_2 (Morris et al., 2011). H_2O_2 is a reactive compound among many factors that creates a stressful environment for *Prochlorococcus* cells by damaging cellular proteins, lipids and DNA (Schieber and Chandel, 2014). Performing an assay to detect ROS-induced crosslinks between RbcL subunits, on the three strains of *Prochlorococcus marinus* under study, will give insight to the cumulative effects of ROS on cellular proteins under various growth conditions.

Purpose

The purpose of the current study is to quantify the growth rates of three *Prochlorococcus* strains; MED4, MIT9313, and SS120 across a matrix of various light levels, spectral ranges, and oxygen regimes. The quantitation of cell growth rate will be investigated by measuring optical density at 680nm (OD680), as a proxy for chlorophyll concentration, and optical density at 720nm (OD720), as a proxy for cell scattering which is driven by cell number, size, and refractile conserve content.

The vertical distribution of *Prochlorococcus* across the water column has been studied at the regional and global scale (Johnson et al., 2006; Moore et al., 1995). These studies have shown clear niche-partitioning of *Prochlorococcus* strains associated with environmental conditions including light intensity, temperature, and nutrient concentration, which has defined current ecotypes. However, the role of oxygen concentrations as a factor influencing the niche-partitioning across *Prochlorococcus* strains is a newly emerging area of phytoplankton research (Bagby and Chisholm, 2015; Lavin et al., 2010). The strains used in this study were chosen because they represent variation in ecotypes across depth in the water column. Therefore, this study will give insight to an understudied factor influencing the distribution patterns of *Prochlorococcus* in marine environments. It is hypothesized that changes in light intensity, colour, and oxygen concentrations will differentially alter the growth and physiological responses of each unique *Prochlorococcus* strain. Furthermore, it is predicted that the highlight ecotype, *Prochlorococcus* MED4, will grow best under high oxygen and high light levels and the lowlight ecotypes, *Prochlorococcus* MIT9313 and *Prochlorococcus* SS120 will grow best under low light regimes.

The results of the current study address foundational elements of climate change by pursuing fundamental biological response mechanisms of a globally critical functional group, the oceanic phytoplankton. Studying the physiological responses of phytoplankton under varying conditions will provide scientific insight to how phytoplankton contribute to marine food webs and the impact environmental conditions have on currents and future environmental niche partitioning of *Prochlorococcus* ecotypes.

Materials and Methods

Species Analyzed

Three strains of *Prochlorococcus marinus* were used throughout this study.

Table 2. Isolation information for *Prochlorococcus* strains used in this study (Campbell and Vaulot, 1993; Moore and Chisholm, 1999)

Strain name	Location	Coordinates	Depth of Isolation	Date isolated	Isolator
MED4	Mediterranean Sea	43.2°N, 6.9°E	5m	January 1989	D. Vaulot
MIT9313	Gulf Stream	37.5°N, 68.2°W	135m	July 1993	L. R. Moore
SS120*	Sargasso Sea	29°N, 64.4°W	120m	May 1988	B. Palenik

*Same strain as CCMP1375

Culture Growth

Leading up to inoculation in a Multi-Cultivator run *Prochlorococcus marinus* MIT9313 and *Prochlorococcus marinus* SS120 were maintained in Pro99 medium, with cycles of 1 in 5 dilution of inoculant (refer to Dropbox link in appendix for media preparation). These Precultures of *Prochlorococcus* MIT9313 and *Prochlorococcus* SS120 were incubated at 22℃ on a cycle of 12 hrs at 30 µmol photons m^{-2} s^{-1} followed by 12 hrs dark.

Prochlorococcus marinus MED4 was maintained in Pro 99 medium with cycles of 1 in 2 dilution of inoculant (refer to Dropbox link in appendix for media preparation). The precultures of *Prochlorococcus* MED4 were incubated at 22℃ on a cycle of 12 hrs at 150 µmol photons m^{-2} s^{-1} followed by 12 hrs dark. Maintaining *Prochlorococcus* MED4 at higher light helps avoid over-growth by the low-light ecotypes.

Each culture was left to grow for one week with daily swirling to reach a high density to be used to inoculate corresponding Multi-Cultivator run.

Multi-Cultivator Unit

Each *Prochlorococcus marinus* strain was pre-cultivated as described above and then diluted to various volumes depending on the predetermined growth experiment protocol. Growth under defined conditions of light level, light color, temperature and O_2 gas concentration was then tracked using Multi-cultivator photobioreactors (serial numbers MCMIX004 and MCMIX006, Photon System Instruments, Brno, Czech Republic) in 80mL glass tubes (40mm) at 22℃ to ensure consistent growth temperature across all strains.

The Multi-Cultivator is an automated unit intended for small scale screening experiments of phototrophic organisms including picocyanobacteria. The unique design of this unit allows a fast comparison among various strains, light intensities, and gas concentrations, while running almost autonomously. The Multi-Cultivator uses two optical density (OD) sensors to record cellular growth under each condition in each tube (Figure 4 (B)). Optical density measured at 680nm (OD680) is a proxy for relative chlorophyll content and cell scattering. Optical density measured at 720nm (OD720) is a proxy for cell scattering alone, dominated by cell suspension density, cell size and cellular content of refractile (Rabouille et al., 2021).

N_2, CO_2 and Oxygen Supply to Cultures

To drive down oxygen saturation some culture tubes were bubbled with a mix of nitrogen gas (N_2) and carbon dioxide (CO_2) flowing at rates of 0.706 N_2 mL m^{-1} and 0.350 CO_2 mL m^{-1} respectively, controlled using digital mass flow controllers (QuBit Systems). This generated a stream of bubbles of ~500 ppm CO_2 in N_2 , distributed to culture tubes through the Multi-Cultivator gas manifold system to drive off dissolved O_2 while delivering CO_2. Other cultures were maintained at full air levels of dissolved oxygen by bubbling with room air, thereby avoiding excess O_2 during illuminated photosynthesis. Some culture runs were monitored with optode O_2 detectors (FireSting, Pyroscience, Germany) to verify the achievement of target concentrations of dissolved O_2 gas concentrations (data not presented).

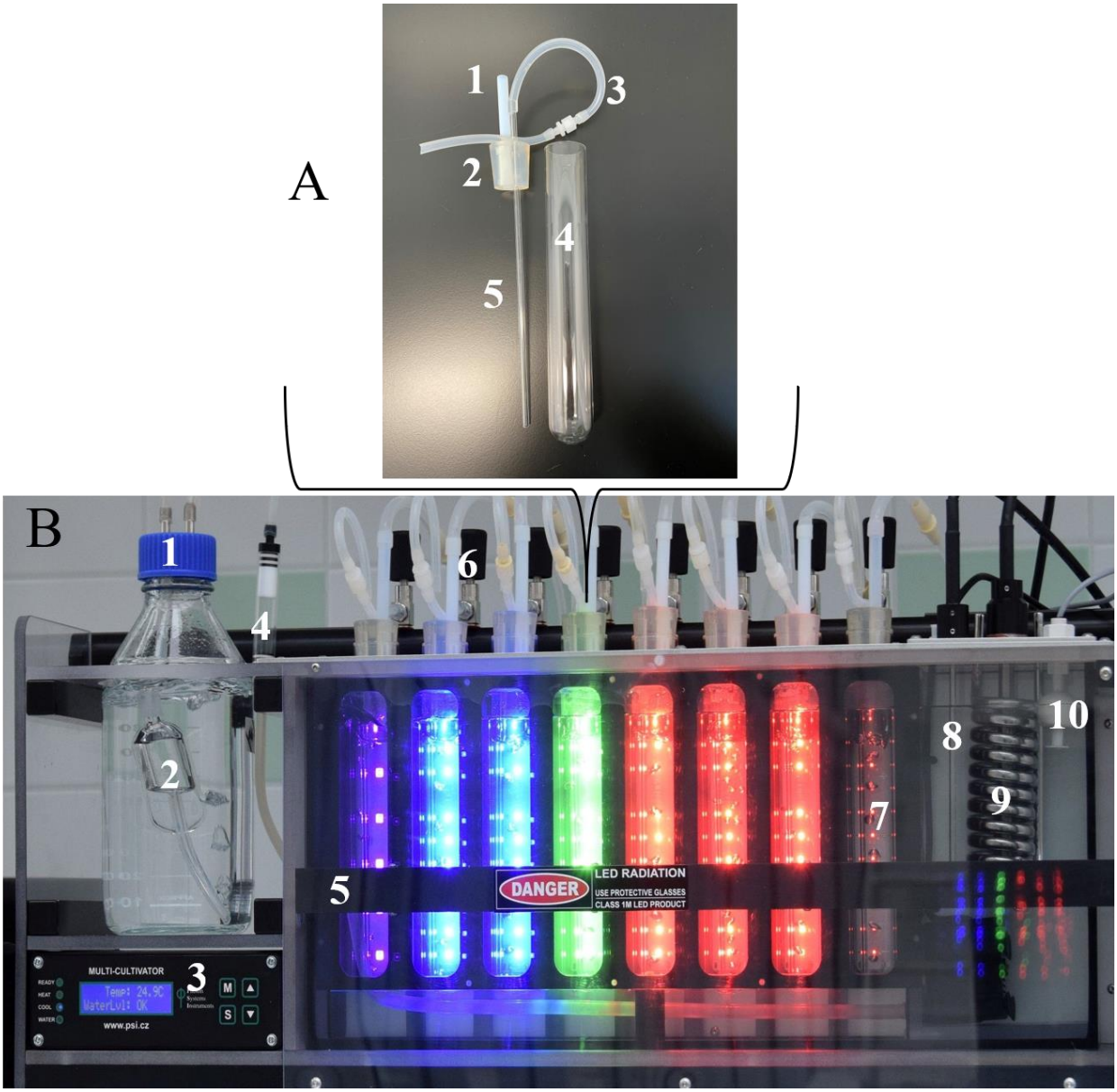

Figure 4. (A) Annotated image of 80mL Multi-Cultivator glass tube **1.** Teflon inoculation tube **2.** Inert silicone stopper **3.** Silicon gas tube **4.** 80mL glass Multi-Cultivator tube **5.** Glass insert delivers gas to the bottom of the tube to suspend cells in media.
(B) Annotated image of Multi-Cultivator unit (Photon Systems Instruments, Brno, Czech Republic) **1.** Bladder cap with gas input and output tubes **2.** Glass bladder regulating gas bubbling into individual tubes. **3.** System control center, allowing the user to set bubble idle intervals, temperature settings, OD calibration and measurements. **4.** Back pressure valve which controls bubble idle. **5.** Optical density (OD) sensor. **6.** Manual dial control for bubble intensity for each individual tube. **7.** LED light panel. **8.** Temperature probe **9.** Heating coil. **10.** Water level sensor.

Pre-run Preparation

As summarized by the green boxes in Figure 5 there are multiple steps to take before starting a Multi-Cultivator run.

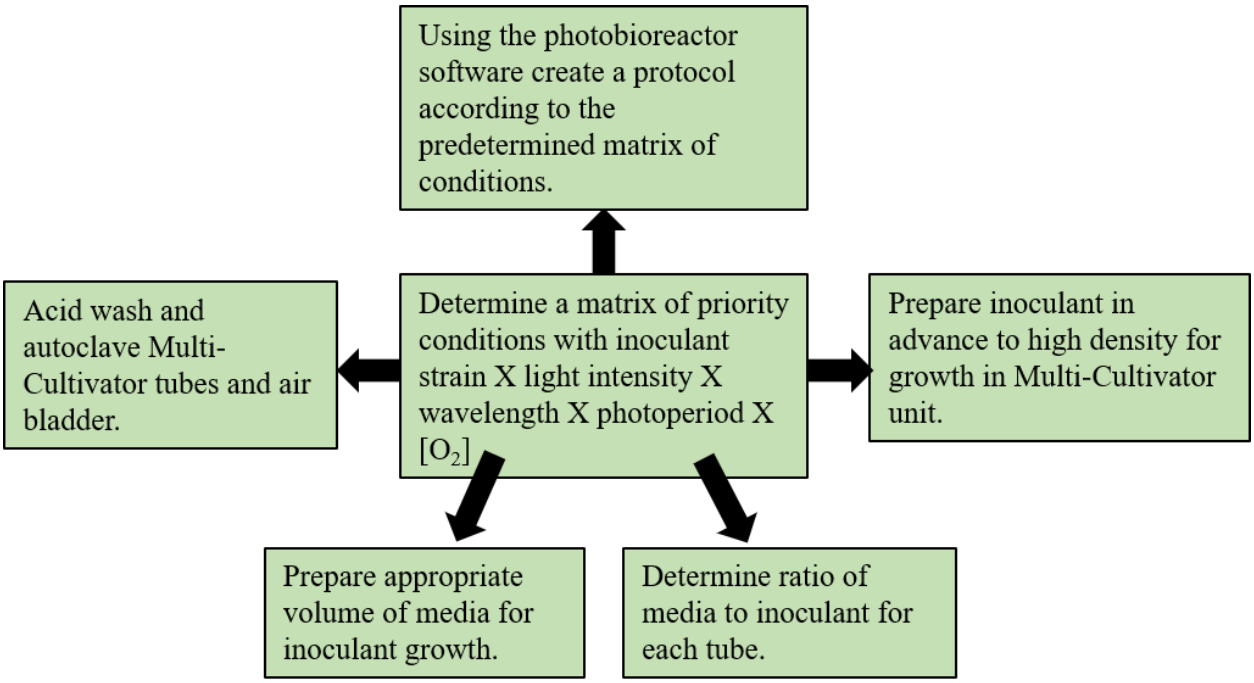

Figure 5. Schematic of procedures and requirements to prepare for a Multi-Cultivator run.

A total of eight 80mL MultiCultivator tubes were acid washed and autoclaved for each run. The glass air bladder (Figure 4, (B)) must be acid washed and autoclaved the day of in preparation for a Multi-Cultivator run. Next, 560mL of Pro99 media was prepared resulting in a 1:7 ratio of media to inoculum for each tube in a run.

I planned a matrix of conditions varying in species, peak light intensity of growth light, wavelength of growth light, photoperiod of growth light, temperature, and oxygen concentration. We then programmed the photobioreactor client software to apply the appropriate conditions to each of 8 tubes per run. The protocol was set to start the run autonomously at a desired start date and time; in my case all growth protocols started at 06:00, after inoculation of tubes the previous afternoon

Day of Run

The steps to start a run are indicated by the orange boxes in Figure 6.

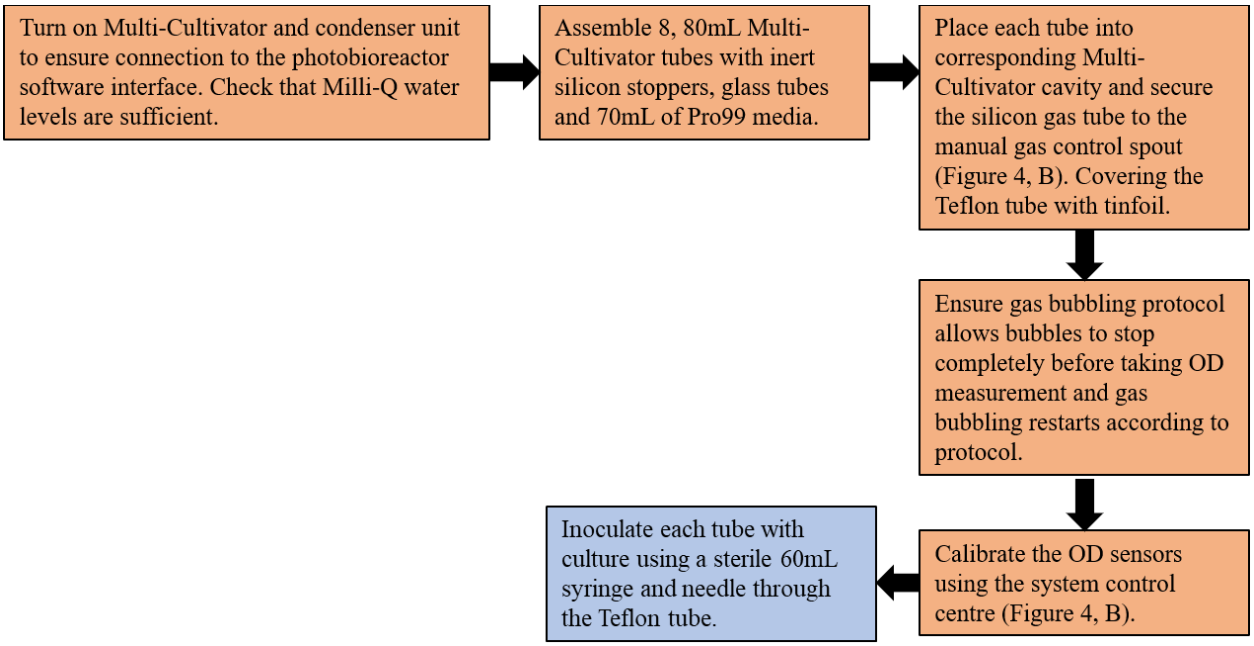

Figure 6. Schematic of procedures performed the day of a run set-up. These actions can only take place after the preparation steps are completed.

First, the Multi-Cultivator unit and condenser were turned on to ensure the connection between the photobioreactor software and the physical unit and to ensure sufficient Milli-Q water level. Next eight, 80mL tubes were assembled with the corresponding inert silicone tube stopper and filled with 70mL of Pro99 media working under a flow hood to minimize contamination. Next, each tube was placed in the Multi-Cultivator cavity and the silicone gas tube was secured to the manual gas spout (Figure 4, (A)) ensuring the teflon tube is covered with tinfoil to reduce contamination. After Multi-Cultivator tubes are inserted and secured to the gas bubbling, the gas bubble idle is checked to ensure bubbling does not interrupt the OD measurements and restarts according to protocol. Next the OD sensors are calibrated using the system control center just before inoculation (Figure 4 (B)). Each tube was then inoculated with 10mL of corresponding culture using a 60mL Luer-Lok™ syringe (Ref No. 309653) and hypodermic needle (Ref No. 8300015029) through the rigid Teflon tube in each Multi-Cultivator glass tube.

Post Inoculation

After inoculation of desired culture there are various steps indicated by Figure 7 to ensure the Multi-Cultivator run successfully captures OD680 and OD720 measurements.

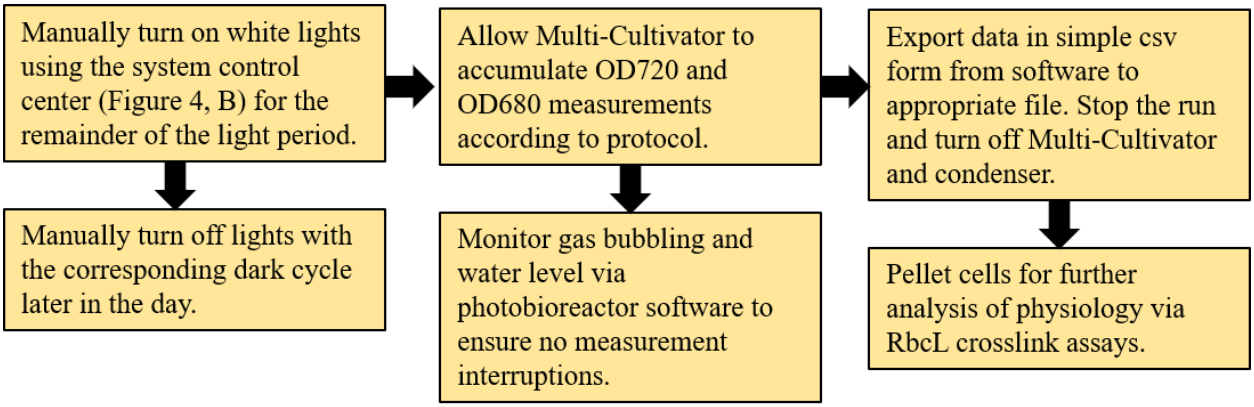

Figure 7. Schematic of procedures post inoculation of Multi-Cultivator run.

After inoculation white lights were manually turned on using the system control center (Figure 4, (B)) for the remainder of the light photoperiod according to protocol. Later, on the first day the white lights are manually shut off in correspondence to the start of the protocol dark photoperiod of 18:00-06:00. As OD680 and OD720 measurements are accumulated autonomously by the Multi-Cultivator unit, the gas bubbling and water level are monitored regularly by the operator to avoid measurement interruptions. Once the protocol has accumulated OD measurements according to the desired length of the protocol the data file is exported in a simple CSV format for the entire length of time. As time elapses and cells begin to grow the cells are harvested from individual tubes and pelletized from some tubes once OD680 measurements reached 0.160-0.399. After the data was exported to computer memory the run was stopped by the photobioreactor client software and by manually shutting off the Multi-Cultivator and condenser unit.

Cell Pelleting

Prochlorococcus MED4, *Prochlorococcus* MIT9313, and *Prochlorococcus* SS120 (80mL of selected culture) were divided into two 50mL Falcon tubes (35mL in each tube) once they reached an optical density 680nm (OD680) measurement ranging between 0.160-0.399. Pluronic acid F-68, 0.01% (v/v final), was added into each Falcon tube to overcome cell-cell repulsion and allow formation of a pellet. The tubes were centrifuged in the Beckman Avanti J-26 XP Centrifuge with a JA-10 rotor (S/N 14U2527) for 10 minutes at 10,000 xg at 4°C. The supernatant in each 50 ml tube was decanted, except for 1.5mL. The remaining supernatant was used to resuspend the pellets with the resulting suspensions transferred into a single 2.0mL Eppendorf tube (Axygen©, MCT-200-C-S) for each original culture sample. The Eppendorf

tubes were subsequently centrifuged at room temperature for 5 minutes at 14,000 xg. The supernatant was discarded from each tube and the pellets were stored at -80°C.

Photobioreactor Growth Plots

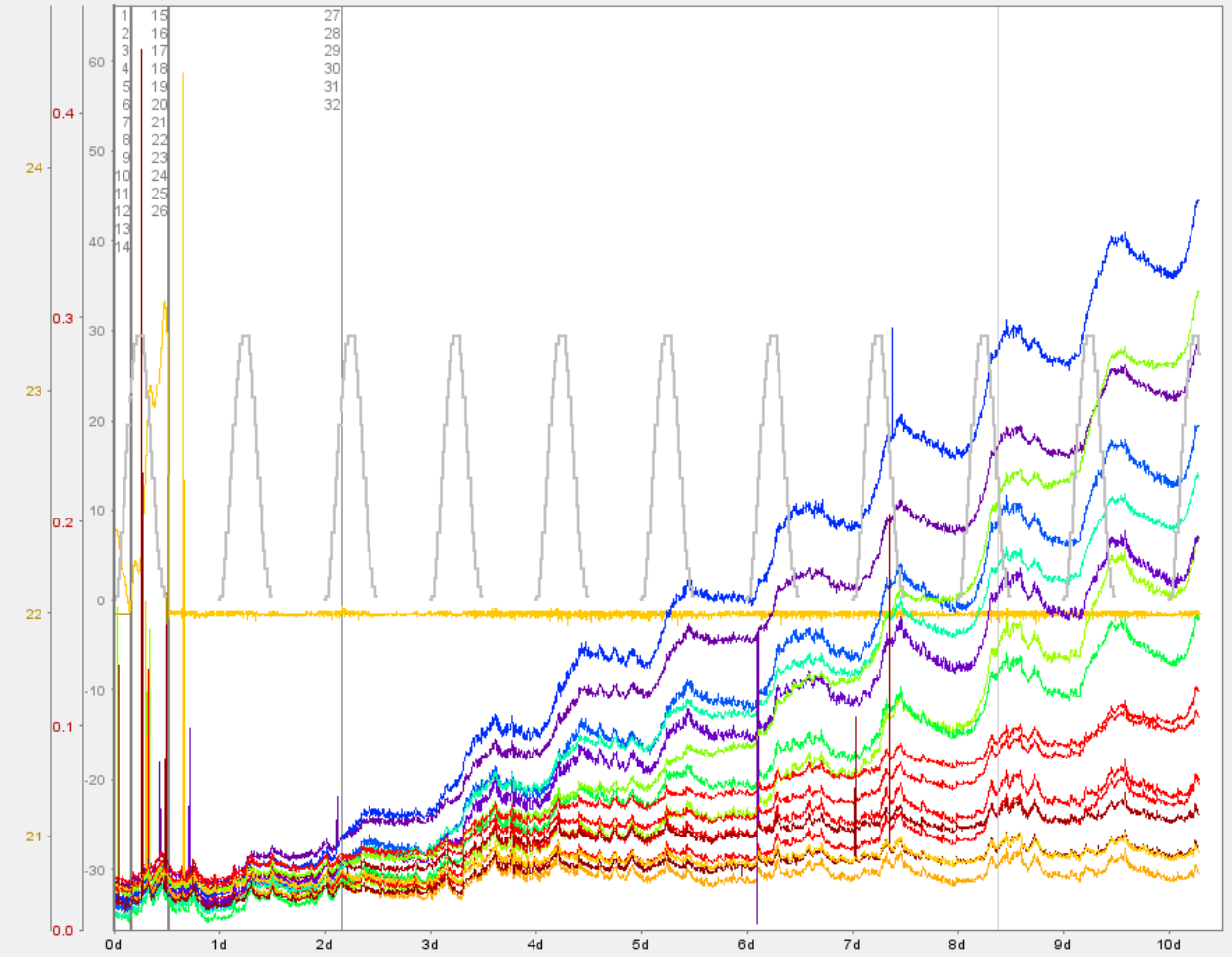

Figure 8. Representative data traces taken from the Bioreactor data capture client software (Photo Systems Instruments, 2016) showing the OD680 and OD720 measurements taken from each of 8 culture tubes, tracking the growth of *Prochlorococcus* MIT9313 or SS120 during a Multi-Cultivator run (colored traces). Note the pronounced diel cycling of OD measures. Grey trace shows illumination for tube 1 following a 12 h photoperiod sine wave peaking at 30 µmol photons m^{-2} s^{-1}, with a 12 h intervening dark period. Horizontal yellow trace shows temperature logging. Screenshot taken at the end of 20200627_PICO_MCMIX006_RUN14.

Figure 8 shows a representative data trace captured over a 10-day growth trajectory for the 8 tubes of a Multi-Cultivator run. OD measures at 680 and 720 nm were captured every 5 min throughout the trajectory, for a total of 5760 measures per tube. In parallel temperature for the bioreactor was monitored continuously and the light levels from each of 8 different potential LED sources providing different wavebands of light to each tube were tracked for each of the 8 tubes approximately every 30 seconds. This generated an output file of ~200 thousand rows of data from each run. During my project I worked with colleagues to capture 24 such Multi-Cultivator runs comprising 192 growth trajectories totaling ~4.8 million rows of data.

Imported and Tidied Optical Density Data

Once data from the Bioreactor data capture client software was exported as a simple .csv to an online Dropbox folder, the report data was imported to R using the 'fread_plus' function (Dowle and Srinivasan, 2019). Figures resulting from these analyses were generated using the 'tidyverse' and 'ggplot2' packages (Wickham, 2017, 2016)

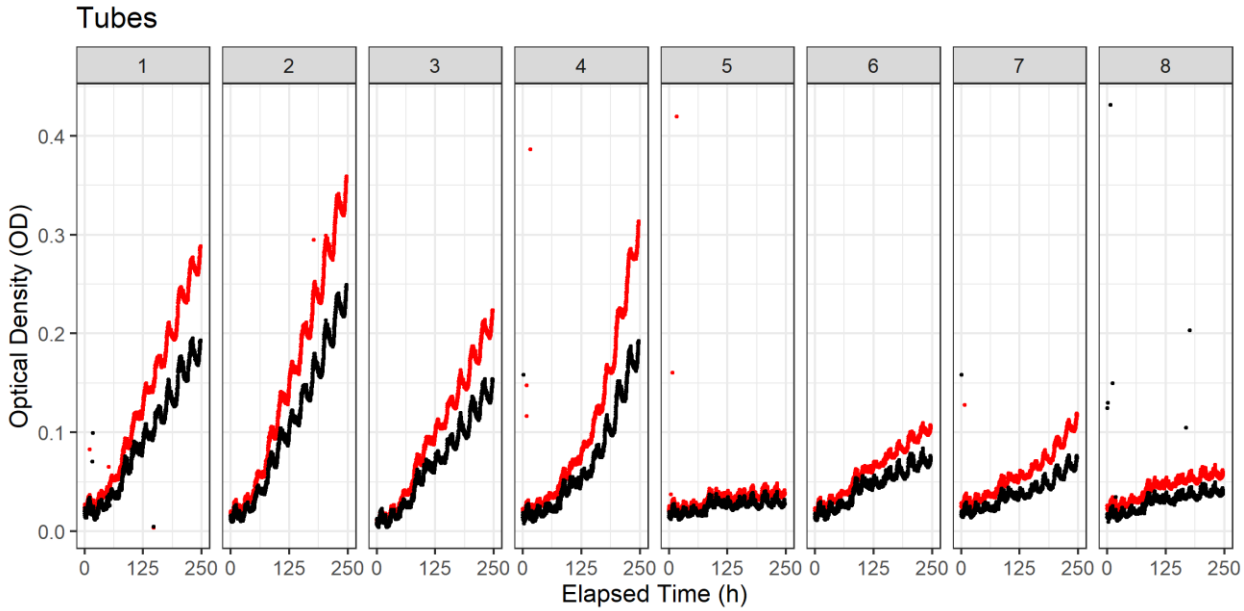

Figure 9. Representative data imported into R and replotted, showing optical density (OD) measurements for 680nm (red trace) and 720nm (black trace), tracking the growth of *Prochlorococcus* SS120 or MIT9313 versus the elapsed time in hours during a Multi-Cultivator run for each of 8 culture tubes, shown as separate facets in this figure. Note the pronounced diel cycling in OD measurements and wide variation in growth trajectories across strains and tubes. Note also sporadic outlier points, usually caused when a gas bubble interfered with the OD measure. Representative data from 20200627_PICO_MCMIX006_RUN14.

Figure 9 shows representative data from a Multi-Cultivator run plotted after being imported into R and faceted by tube number. This plot shows data before filtering data outliers and merging with the MetaData catalog containing environmental descriptions of the cultures run in each tube. The data outliers are evident in the OD680 and OD720 traces seen in Figure 9 represented by the scattered black and red points above the prominent data traces. These outliers usually occur when a gas bubble interferes with the measurement of optical density. Also note a step-change in OD around 100 h across tubes in this run, which likely results from an electronic offset in the baseline signal, since it is unlikely that a biological signal would align so closely across all eight tubes.

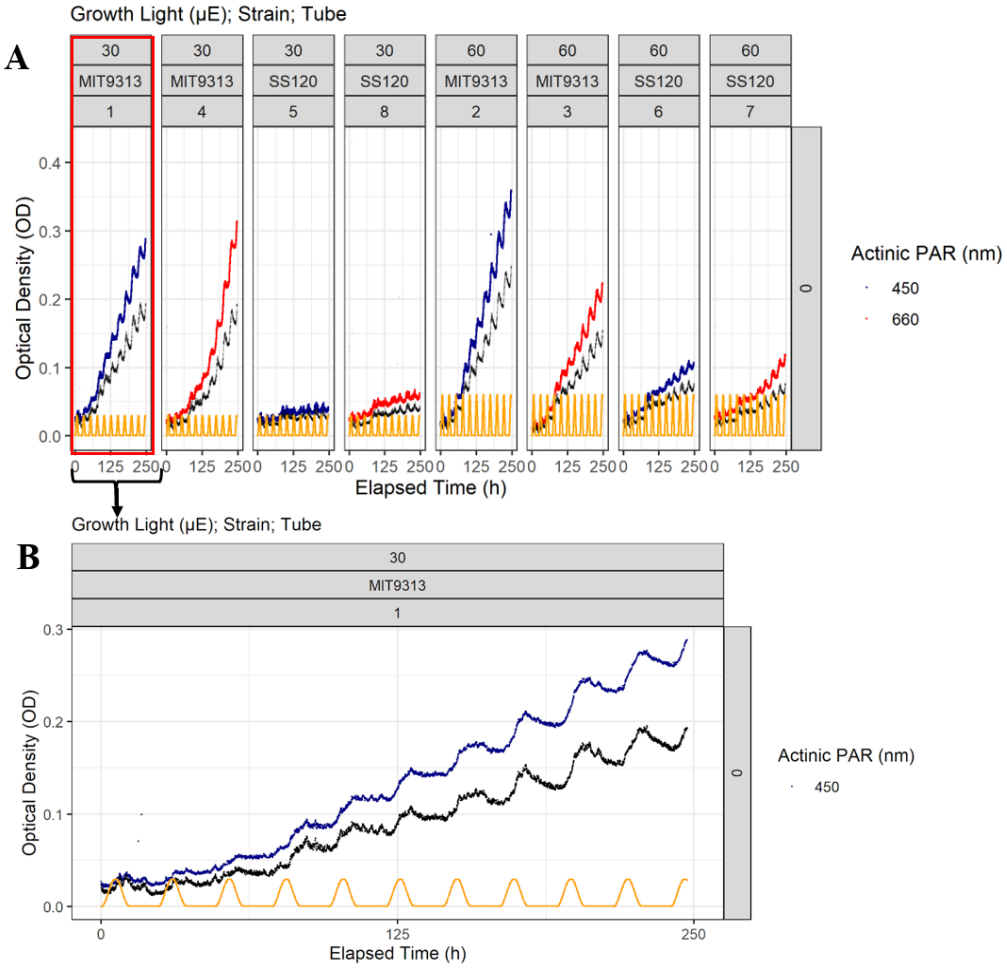

Figure 10. (A) Representative data after filtering of outliers, showing optical density at 680nm (OD680) tracking the chlorophyll and cell scattering of *Prochlorococcus* MIT9313 and SS120 strains growing under 450nm (blue traces) or 660nm (red traces) light over the elapsed time in hours during a Multi-Cultivator run for each of the 8 culture tubes. Black traces show parallel measures of optical density at 720nm (OD720) tracking cell density for each tube. Plot is faceted by growth light level (µmol photons m^{-2} s^{-1}), Strain and culture tube number. Yellow trace shows illumination (divided by 1000 for scaling of Y axis) for each tube following a 12h photoperiod sine wave peaking at 30 µmol photons m^{-2} s^{-1} (tubes 1, 4, 5, and 8) and 60 µmol photons m^{-2} s^{-1} (tubes 2, 3, 6, 7), with a 12h intervening dark period. All tubes were maintained at near 0 dissolved oxygen by continuous sparging with an N_2/CO_2 gas mix, indicated by the '0' beside the row of panels. Note the elimination of most (not all) outlier points at the cost of loss of some good data points shown by gaps in some data traces.
(B) Representative filtered data expanding OD680 (blue trace) and OD720 (black trace) measurements from a single tube, for *Prochlorococcus* MIT9313 growing under 450nm and near-0 dissolved oxygen. Yellow trace shows illumination for tube 1 following a 12h photoperiod sine wave peaking at 30 µmol photons m^{-2} s^{-1}. Illumination values divided by 1000 for Y axis scaling. Note the small break in data trace for OD680 at approximately 190h, resulting from filtering of outlier values that usually result when a bubble interferes with a measurement. Representative data from 20200627_PICO_MCMIX006_RUN14.

Figure 10 shows representative data filtered and merged with the MetaData catalog for *Prochlorococcus* MIT9313 and SS120. Using RStudio running 'tidyverse' (Wickham, 2017) and interpolation (Guerrero, 2014) functions a column containing values of µmol photons m^{-2} s^{-1} was interpolated to correspond temporally with the corresponding OD measurements at the given time points within a run. Then using pivot_wider (Wickham, 2017) the long-format representative data file was flipped to wide format to align the appropriate actinic light column values with relevant OD column measurement data. The MetaData catalog contains the manually entered values for the matrix of strain, light and oxygen regimes for each tube of each run.

The data plotted in Figure 10 was filtered using a moving average window in RStudio looking at 50 sequential data points from a given OD data column at a time. Any data points that were over 1.5X the running average of the 50-point window were flagged for exclusion. This method of filtering became problematic when multiple bubble interruptions occurred within a small time frame causing a cluster of outlying data points. This was overcome by adjusting the moving average window to be shorter to better suit the duration of bubble interruptions and corresponding false OD measurements.

Results

Once data from each run was filtered for outliers, merged with MetaData, and the actinic light was interpolated an interval of data was selected to implement a logistic regression mode of OD720 and deltaOD for each environmental condition. The logistic regression models were plotted to compare the response to different environmental conditions in terms of chlorophyll accumulation per mL (OD680-OD720, deltaOD), cell scattering and cell suspension density (OD720). Although we were able to qualitatively compare growth rates and physiological differences between strains the next step in this project is to complete statistical tests to quantitatively discuss the results generated from this project.

Logistic Regression Model

To explore the sustained growth responses of *Prochlorococcus marinus* to varying environmental conditions logistic regression models were fitted across the entire run, resulting in 192 unique Pmax estimates, intercepts, and growth rates for each tube. Nonlinear regressions were predicted using a logistic_eqn function in R which is defined below (Elzhov et al., 2016; Wickham, 2017). The starting, lower and upper bounds for the fit parameters were defined to constrain the logistic fit. The logistic model was fit for OD720, tracking cell suspension density and scattering; and deltaOD (OD680-OD720) tracking chlorophyll accumulation per mL across the entire run.

$$OD720\ or\ deltaOD = \frac{Pmax \times Intercept^{(mu(x))}}{Pmax + (Intercept^{(mu(x)-1)})}$$

Table 3. Starting, lower, and upper logistic equation parameter values defined to constrain the logistic fit.

	Starting parameter values	Lower parameter values	Upper parameter values
Pmax	0.3	0.1	0.5
mu	0.01	-0.1	0.1
intercept	0.01	0.001	0.1

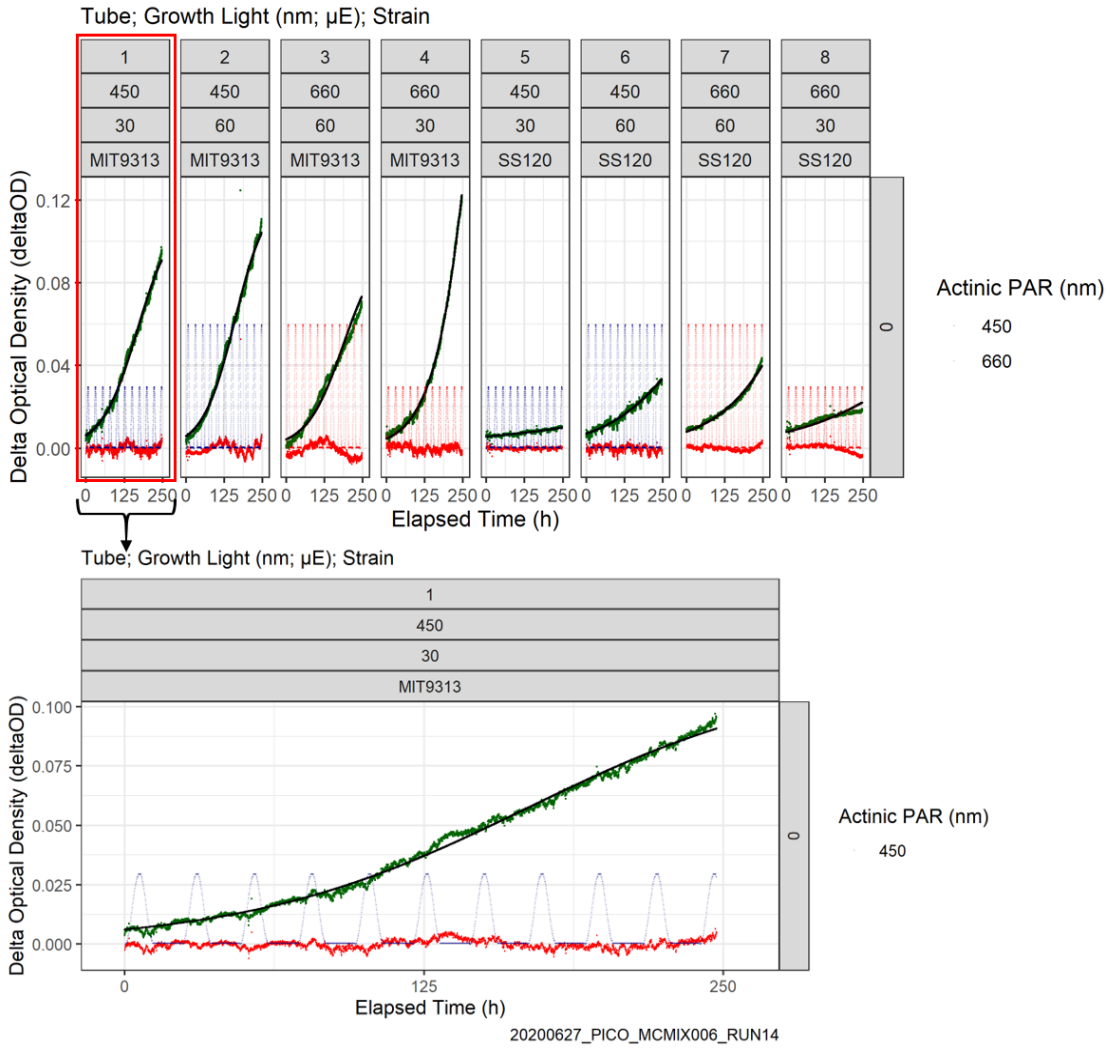

Figure 11. (A) Representative data after filtering of outliers, showing delta optical density (deltaOD) tracking the chlorophyll accumulation of *Prochlorococcus* MIT9313 and SS120 strains (green traces) growing under 450nm (blue traces) or 660nm (red traces) light over the elapsed time in hours during a Multi-Cultivator run for each of the 8 culture tubes. Black traces show the prediction of the logistic model fit for each tube. Dark red traces show the residuals of the logistic model. Plot is faceted by culture tube number, growth light wavelength, growth light level (µmol photons m^{-2} s^{-1}) and Strain. Tubes 1, 4, 5, and 8 show illumination (divided by 1000 for scaling) peaking at 30 µmol photons m^{-2} s^{-1}, with a 12h intervening dark period. Tubes 2, 3, 6, and 7 show illumination (divided by 1000 for scaling on Y axis) peaking at 60 µmol photons m^{-2} s^{-1}, with a 12h intervening dark period. All tubes were maintained at near 0 dissolved oxygen by continuous sparging with an N_2/CO_2 gas mix, indicated by the '0' beside the row of panels.
(B) Representative filtered data expanding deltaOD (green trace) measurements from a single tube, for *Prochlorococcus* MIT9313 growing under 450nm. Blue trace shows illumination at 450nm for tube 1 following a 12h photoperiod sine wave peaking at 30 µmol photons m^{-2} s^{-1}, with a 12h intervening dark period. Black trace shows the logistic fit of the tube predicted by a logistic equation over the entire data set. Red trace shows the residuals from the logistic model. (Representative data from 20200627_PICO_MCMIX006_RUN14).

Figure 11 shows a logistic regression model with residuals plotted for deltaOD for each tube across an entire representative run faceted into panels by tube, growth light (µE), and strain. The logistic regression predictions were analyzed for each tube across all runs resulting in 192 separate Pmax estimates and intercepts based upon our proxy for chlorophyll ml^{-1}, deltaOD. Figure 11 shows an accumulation of chlorophyll mL^{-1} in most tubes as time elapses, chlorophyll ml^{-1}shows little to no cyclic pattern following the growth light sine wave progressions.

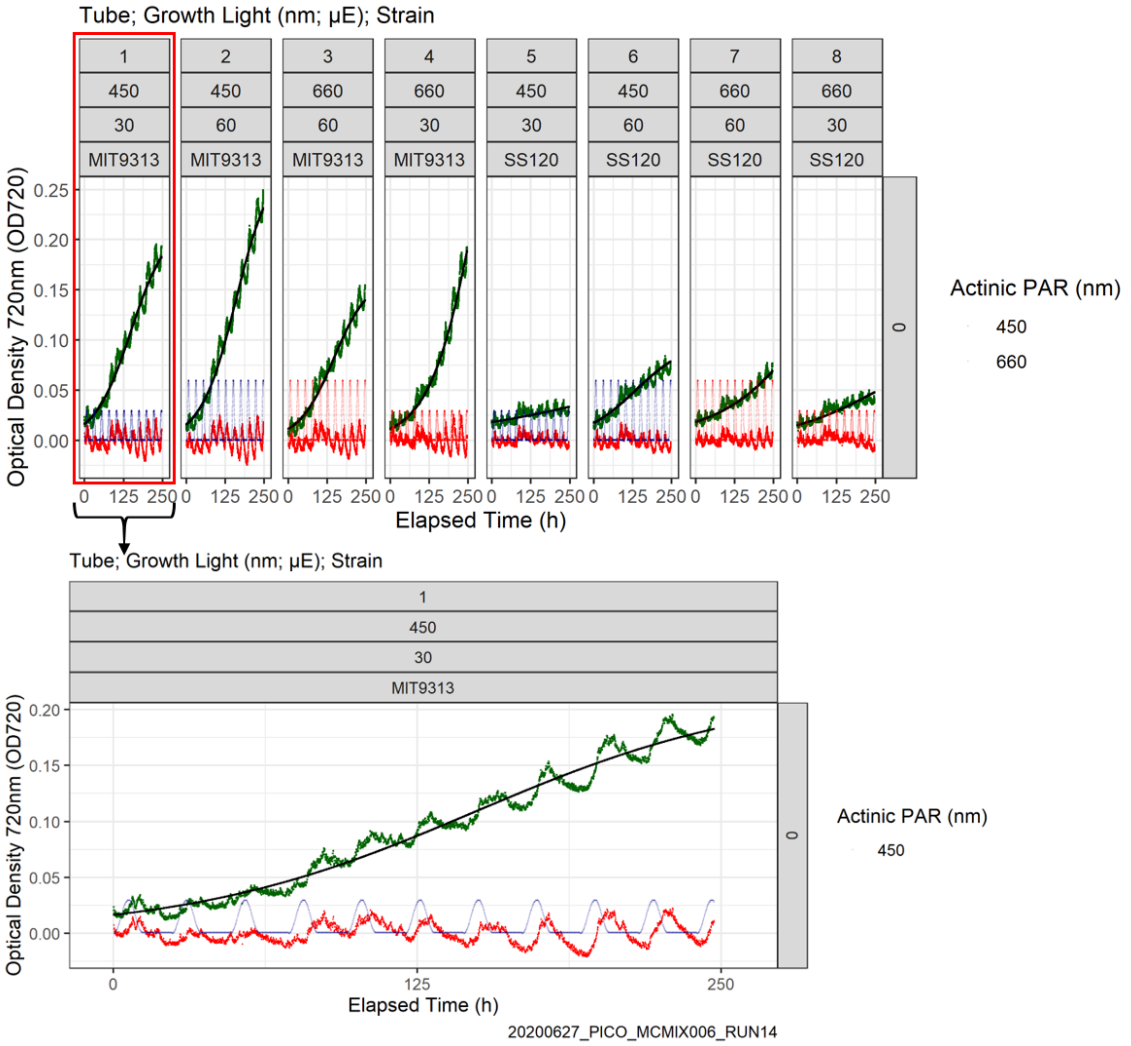

Figure 12. (A) Representative interval data after filtering of outliers, showing the optical density at 720nm (OD720) tracking the cell density, cell size and scattering related to carbohydrate reserves of *Prochlorococcus* MIT9313 and SS120 strains (green traces) growing under 450nm (blue traces) or 660nm (red traces) light over the elapsed time in hours during a Multi-Cultivator run for each of the 8 culture tubes. Black traces show the prediction from a logistic model fit for each tube Dark red traces show the residuals of the logistic model. Plot is faceted by culture tube number, growth light wavelength, growth light level (µmol photons m^{-2} s^{-1}) and Strain. Tubes 1, 4, 5, and 8 show illumination (divided by 1000 for scaling on the Y axis) peaking at 30 µmol photons m^{-2} s^{-1}, with a 12h intervening dark period. Tubes 2, 3, 6, and 7 show illumination (divided by 1000 for scaling on the Y axis) peaking at 60 µmol photons m^{-2} s^{-1}, with a 12h intervening dark period. All tubes were maintained at near 0 dissolved oxygen by continuous sparging with an N_2/CO_2 gas mix, indicated by the '0' beside the row of panels.
(B) Representative filtered data expanding deltaOD (green trace) measurements from a single tube, for *Prochlorococcus* MIT9313 growing under 450nm. Blue trace shows illumination at 450nm for tube 1 following a 12h photoperiod sine wave peaking at 30 µmol photons m^{-2} s^{-1}, with a 12h intervening dark period. Black trace shows the logistic fit of the tube predicted by a logistic equation over the entire data set. Red trace shows the residuals from the logistic model. (Representative data from 20200627_PICO_MCMIX006_RUN14).

Figure 12 shows a logistic regression model with residuals for OD720 for each tube across an entire representative faceted by tube, growth light (µE), and strain. The logistic regression predictions were analyzed for each tube across all runs resulting in 192 separate Pmax estimates and intercepts based upon our proxy for cell scattering, OD720. This plot shows pronounced diel cycling in cell scattering that follows the fluctuating light level across a 12h sine wave progression, with a shift in the phase of the fluctuations.

Summary Growth Plots

To compare the growth rates and physiological responses to varying growth regimes across all three strains in this study the logistic fit terms were extracted from the tube-specific fits of the logistic equation to create a summary table of the growth rates based upon chlorophyll and cell scattering for each tube across each run.

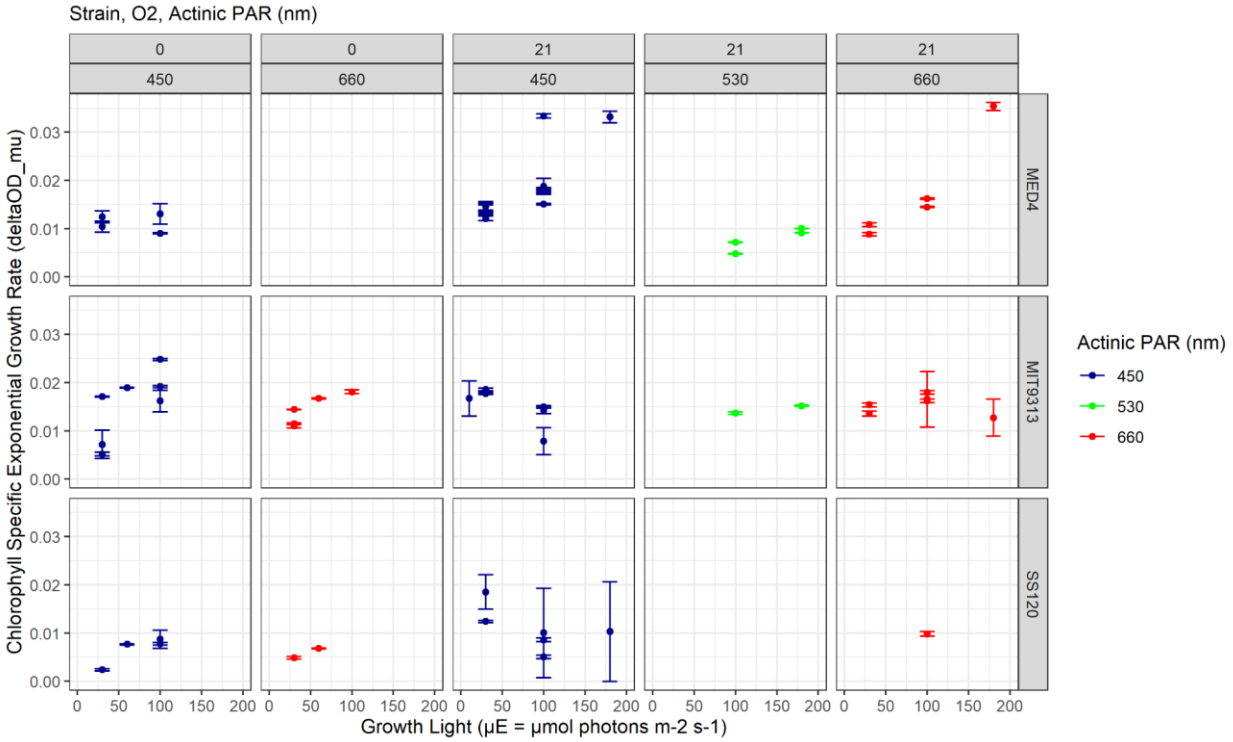

Figure 13. Chlorophyll specific exponential growth rate (deltaOD_mu) plotted against growth light (µmol photons $m^{-2}s^{-1}$) tracking the accumulation of chlorophyll mL^{-1} of *Prochlorococcus* MED4, MIT9313, and SS120 strains growing under 450nm (blue points), 660nm (red points), or 530nm (green points) light. Growth light (µmol photons m^{-2} s^{-1}) followed a 12h sine wave peaking at the light level plotted on the X axis, followed by a 12h intervening dark period for all runs. Error bars are defined as the standard error of the fitted term, in this case deltaOD_mu. All tubes were maintained at near 0% dissolved oxygen or 21% air saturation by continuous sparging with an N_2/CO_2 gas mix and room air respectively indicated by the '0' or '21' for each column of facet panels.

In Figure 13 *Prochlorococcus* MED4 has the highest chlorophyll specific exponential growth rates at 21% oxygen saturation under blue (450nm) and red (660nm) light peaking at 180 µmol photons m^{-2} s^{-1}. There is also a positive trend as peak illumination levels increase which was expected as MED4 is deemed a high light ecotype (Figure 13). *Prochlorococcus* SS120 also showed high chlorophyll specific exponential growth rates at 0% oxygen saturation under blue (450nm) and red (660nm) light peaking at 60 and 100 µmol photons m^{-2} s^{-1} (Figure 13). *Prochlorococcus* MIT9313 showed the highest exponential growth rate for chlorophyll at 0% oxygen saturation under blue (450nm) and red (660nm) light peaking at 100 µmol photons m^{-2} s^{-1} (Figure 13).

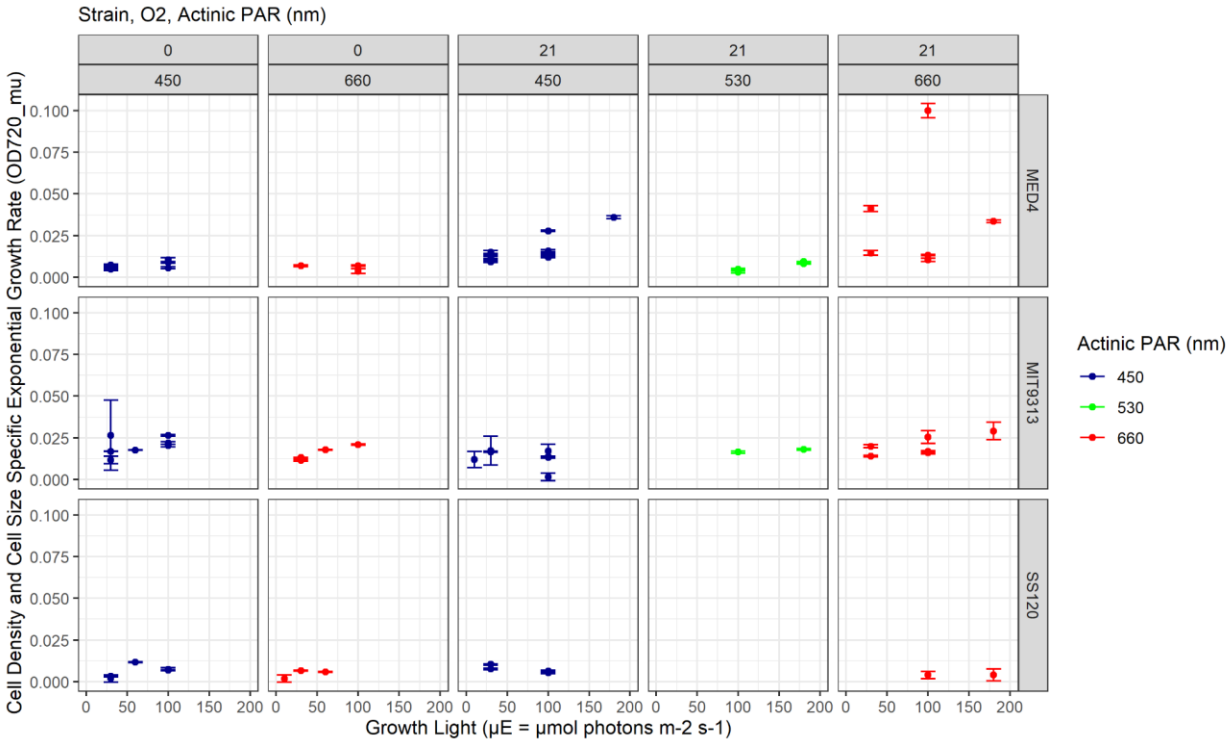

Figure 14. Cell density and cell size specific exponential growth rate (OD720_mu) plotted against growth light (µmol photons $m^{-2}s^{-1}$) tracking cell scattering, which is driven by cell suspension density, cell size and scattering related to carbohydrate reserves of *Prochlorococcus* MED4, MIT9313, and SS120 strains, growing under 450nm (blue points), 660nm (red points), or 530nm (green points) lights. Growth light (µmol photons m^{-2} s^{-1}) followed a 12h sine wave peaking at the light level plotted on the X axis followed by a 12h intervening dark period for all runs. Error bars are defined as the standard error of the fitted term, in this case OD720_mu. All tubes were maintained at near 0% dissolved oxygen or 21% air saturation by continuous sparging with an N_2/CO_2 gas mix and room air respectively, indicated by the '0' or '21' for each column of facet panels.

In Figure 14 *Prochlorococcus* MED4 has the highest cell density/size exponential growth rates at 21% oxygen saturation under blue (450nm) and red (660nm) light peaking at 180 µmol photons m^{-2} s^{-1}. *Prochlorococcus* SS120 has the highest exponential growth rate for cell density/cell size at 0% oxygen saturation under blue (450nm) light peaking at 60 µmol photons m^{-2} s^{-1} (Figure 14). *Prochlorococcus* MIT9313 showed the highest exponential growth rate for cell density/size at 0% and 21% oxygen saturation under blue (450nm) and red (660nm) light peaking at 100 and 180 µmol photons m^{-2} s^{-1} respectively (Figure 14).

To visualize the balance between chlorophyll accumulation and cell density, a plot was generated using the extracted growth rates from deltaOD_mu and OD720_mu for each tube from each run (Figure 15). This plot shows whether the growth rates for two different cell components are the same. If growth rates are balanced the points on the plot will follow a 1:1 linear

relationship. If the growth rates are unbalanced there will be no linear relationship between the two growth rates, which in turn gives insight to how the physiology of *Prochlorococcus* cells are progressively changing in cellular composition over generations.

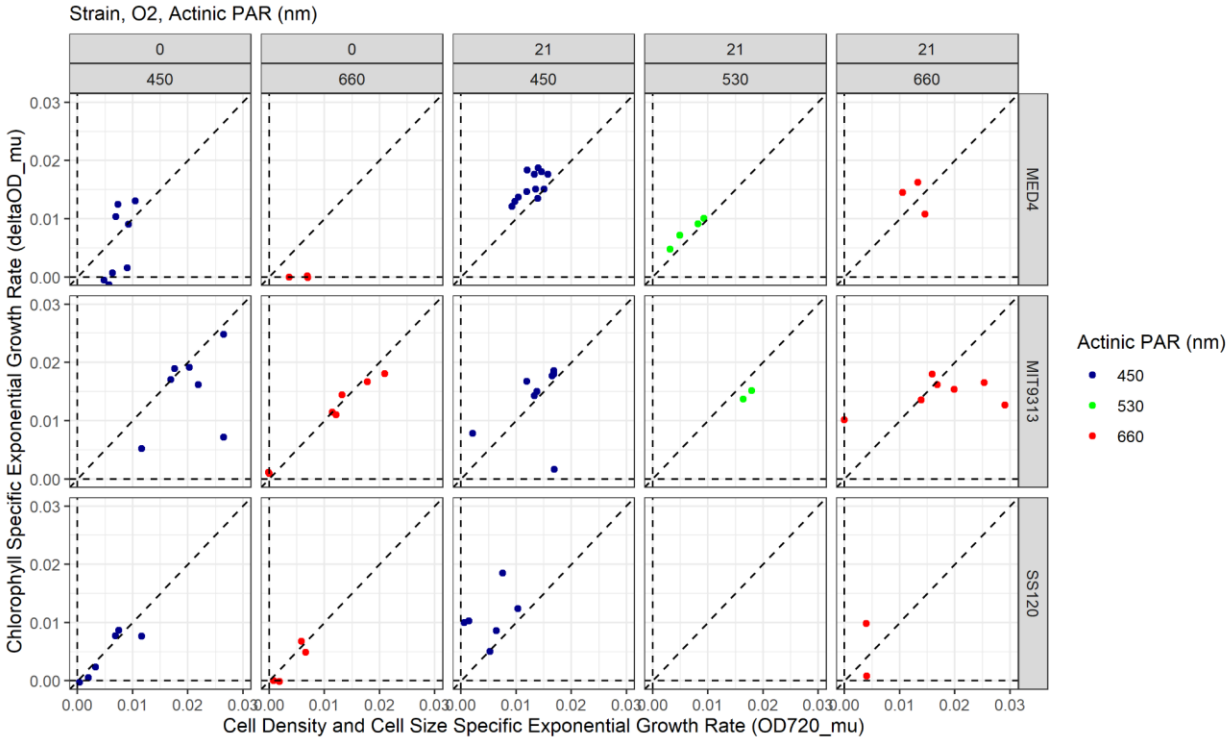

Figure 15. Chlorophyll specific exponential growth rate (deltaOD_mu) plotted against the cell density and cell size specific exponential growth rate (OD720_mu) representing the relationship between two growth rates of *Prochlorococcus* MED4, MIT9313, and SS120 strains growing under 450nm (blue points), 660nm (red points), or 530nm (green points) light. Growth light (µmol photons m^{-2} s^{-1}) followed a 12h sine wave peaking at the light level plotted on the X axis followed by a 12h intervening dark period for all runs. The diagonal dotted line represents a 1:1 ratio expected for balanced growth rates between two different cellular components. All tubes were maintained at near 0% dissolved oxygen or 21% air saturation by continuous sparging with an N_2/CO_2 gas mix and room air respectively, indicated by the '0' or '21' for each column of facet panels.

In Figure 15 *Prochlorococcus* MED4 shows balanced growth at 21% oxygen saturation under blue (450nm) and green (430nm) light. *Prochlorococcus* MIT9313 shows the most balanced growth at 0% oxygen saturation under red (660nm) light and *Prochlorococcus* SS120 shows balanced growth at 0% oxygen saturation under red (660nm) and blue (450nm) light (Figure 15).

Discussion

Changes in chlorophyll, cell abundance and cell composition are visualized by monitoring deltaOD (OD680 - OD720) and OD720. Figures 11 and 12 show the high frequency data obtained from the optical density sensors within the Multi-Cultivator units. Typically, in any given culture, OD rises as biomass increases with increasing time. In the following discussion I describe growth processes that are shorter than the cell division cycle, which result in changes to the N and C composition within the cell, which affect the pattern of the OD signal vs. time. These cellular processes include carbon incorporation, carbon consumption through respiration, and biomass buildup from reserves. Therefore the "growth rates" that are described below encompass all of these processes to some extent.

Diel cyclic patterns in Cell Scattering (OD720)

Plotting the OD720 against elapsed time of the Multicultivator over the entire run gave a visualization of proportional changes in cell density as a response to fluctuating growth light levels (Figure 12). As illumination levels change along a 12h sine wave trajectory the OD720 also increases and decreases following the illumination sine wave pattern with a lag in response time. This pattern is explicable, as distribution of *Prochlorococcus* is structured by a combination of environmental variables, notably irradiance (Larkin et al., 2016). Figure 12 shows that OD720 measurements are closely related to fluctuations in growth light levels but the cells are not affected immediately. This pronounced diel cycling and lag in response time can be explained by the time it takes for the cells to reallocate specific gene expression when transitioning between photosynthesis during the light period and an increase in catabolic consumption of carbohydrate reserves during the dark period (Zinser et al., 2009).

Although OD720 is used as a proxy for cell suspension density it is actually a convolution of cell density, cell size, and content of refractile reserves of carbohydrates which scatter light. For instance, apparent negative growth rates in the early dark phase could be related to the significant consumption of carbon reserves to fuel cellular respiration, leading to a decrease in overall carbon biomass in the culture and hence in OD720 measurements (Rabouille et al., 2021).

Another explanation for fluctuation in OD720 could be attributed to cellular processes during the light phase. At the onset of the light phase there is a rapid increase of OD720 because of photosynthetic processes and photosynthetic oxygen evolution driving carbohydrate accumulation, initiated by the increase in light level.

When comparing these diel cyclic patterns across all three strains and environmental conditions it was qualitatively evident there were no obvious differences among the strains in cellular responses in terms of the pronounced diel cycling patterns seen in Figure 12. Therefore,

cellular processes including respiration and photosynthesis manifest a cyclic pattern in response to growth light across multiple growth conditions. Time series analyses of the strain responses to fluctuating light under different growth conditions are the next step for this project.

Smooth accumulation of Chlorophyll (deltaOD)

In contrast to the fluctuating accumulation of OD720 measurements, plotting deltaOD against elapsed time for each tube over the entire run did not show a pronounced diel cycling of deltaOD measurements (Figure 11). Interestingly, the accumulation of deltaOD measurements as a proxy for chlorophyll shows a smooth trajectory even as illumination levels fluctuate along a 12h sine wave.

Cyanobacteria feature excitation energy transfer among photosynthetic reaction centres for distribution of absorbed light among photosystems to regulate photosynthetic processes. The regulatory processes interact to cause changes in photochemicals and Chl *a* fluorescence yields depending on light and metabolic conditions (Meunier et al., 1998). Therefore, the smooth accumulation of deltaOD measurements demonstrates that although light availability is the proximal factor regulating photosynthesis rates, the photo physiology of *Prochlorococcus* is continuously acclimating over the diel cycle between light and/or dark cycle to maintain balance between light availability and efficiency of chlorophyll utilization.

Patterns of Growth Rates Across Matrix of Conditions

Plotting the chlorophyll specific exponential growth rate (deltaOD_mu) and cell density/cell size specific exponential growth rate (OD720_mu) compared across all tubes from each environmental condition gives insight to the varying growth responses across *Prochlorococcus* strains (Figure 13 and 14). Studying deltaOD_mu as a proxy for chlorophyll is important in this study because the accumulation of chlorophyll represents the efficiency of photosynthetic processes within the cell. The value of OD720_mu as a proxy for cell specific growth rate which allows us to qualitatively study the overlying influences of changes in cell size and cell carbohydrate composition between strains under varying conditions.

In Figure 13 and 14 *Prochlorococcus* MED4 has the highest chlorophyll specific and cell density/size growth rates at 21% oxygen saturation under blue (450nm) and red (660nm) light peaking at 180 µmol photons m^{-2} s^{-1}. There is also a positive trend as peak illumination levels increase which was expected as MED4 is deemed a high light ecotype (Figure 13). This accumulation of chlorophyll under high growth light could be explained by the adaptation of the evolution of Chl-binding proteins to fit divinyl chlorophyll in order to avoid severe photodamage (Ito and Tanaka, 2011). Interestingly, there is an unusually high cell density/cell size exponential growth rate for MED4 at 21% oxygen saturation under red (660nm) light peaking at 100 µmol photons m^{-2} s^{-1} (Figure 14). This high growth rate could be explained by bubble interruptions

during data collection causing extremely high values of OD measurements, poor filtration of data outliers or a higher starting concentration of inoculant in the Multi-Cultivator unit compared to other tubes.

Prochlorococcus SS120 also showed trends of chlorophyll and cell density/cell size growth rates that coincide with the term low light ecotype. *Prochlorococcus* SS120 has the highest exponential growth rate for chlorophyll at 0% oxygen saturation under blue (450nm) and red (660nm) light peaking at 60 and 100 µmol photons m^{-2} s^{-1} (Figure 13). SS120 has the highest exponential growth rate for cell density/cell size at 0% oxygen saturation under blue (450nm) light peaking at 60 µmol photons m^{-2} s^{-1} (Figure 14). The high exponential growth rates under low oxygen saturation and relatively low growth light could be explained by the unique photosynthetic system in *Prochlorococcus marinus* that uses divinyl chlorophyll instead of monovinyl chlorophyll allowing *Prochlorococcus* to harvest blue light more efficiently and grow deeper in the water column, where blue light dominates (Ito and Tanaka, 2011). Figure 13 also shows high rates of chlorophyll specific exponential growth rates for *Prochlorococcus* SS120 at 21% oxygen saturation under blue (450nm) light with large error bars. This variability could be due to high volumes of bubble interruptions causing unusually high measurements in optical density to be missed during filtration of data points.

Prochlorococcus MIT9313 showed the highest exponential growth rate for chlorophyll (detaOD_mu) and cell density/size (OD720_mu) at 0% oxygen saturation under blue (450nm) and red (660nm) light peaking at 100 µmol photons m^{-2} s^{-1} (Figure 13 and 14). These environmental conditions do not naturally occur in marine environments. The reason why *Prochlorococcus* MIT9313 thrives under these conditions could be that genetic expression has made this low light ecotype grow efficiently under low oxygen regimes by utilizing the light and harvesting it to use in photosynthesis to accumulate chlorophyll.

It should also be noted that *Prochlorococcus* MIT9313 has a high exponential growth rate for cell density/size (OD720_mu) when grown at 21% oxygen saturation under red (660nm) light peaking at 180 µmol photons m^{-2} s^{-1} (Figure 14). This could be attributed to the oxygen saturation influencing the cellular processes affecting the content of refractile reserves of carbohydrates which scatter light, increasing optical density measurements.

Further research comparing the growth rates across a matrix of conditions should implement a statistical comparison test to determine the significance between exponential growth rates under varying conditions for each strain. Statistical tests were unable to be completed for this project due to the constraints of memory while working with multiple large data files at once.

Balanced Growth

Plotting the chlorophyll specific exponential growth rate (deltaOD_mu) against the cell density and cell size specific exponential growth rate (OD720_mu) gave a proxy for balanced growth (Figure 15). Plotting two exponential growth rates for two different cellular components visualizes whether growth rates are the same, resulting in balanced growth, or different, showing progressive change in cellular composition over generations.

Prochlorococcus MED4 shows balanced growth at 21% oxygen saturation under blue (450nm) and green (430nm) light (Figure 15). *Prochlorococcus* MIT9313 shows the most balanced growth at 0% oxygen saturation under red (660nm) light (Figure 15). *Prochlorococcus* SS120 shows balanced growth at 0% oxygen saturation under red (660nm) and blue (450nm) light (Figure 15). Balanced growth indicates that over generations of cellular division the exponential growth rate of chlorophyll is proportional to the exponential growth rate of cell density/size as a 1:1 ratio signifying that the cells are ‘acclimated’ to the growth environment.

In some cases, exponential growth rates were not balanced for both cellular components, signifying that there are changes in cellular processes over generations of cell division (Figure 18). The low light ecotypes *Prochlorococcus* MIT9313 and SS120 exhibit unbalanced growth at 21% oxygen saturation under red (660nm) and blue (450nm) light (Figure 18). The high light ecotype *Prochlorococcus* MED4 exhibits unbalanced growth rates at 0% oxygen saturation under red (660nm) and blue (450nm) light. This signifies that oxygen saturation may have an impact on the cellular processes influencing cell size and cell carbohydrate reserves over generations.

Overall, studying two unique growth rates representing separate cellular components has given scientific insight to the diel cyclic patterns of cell scattering and the contrasting smooth accumulation of chlorophyll. In addition to these interesting growth patterns, we were able to visualize and compare these two growth rates against each other to further understand how cellular processes impact each other when exposed to varying environmental regimes.

Implications of this research

Although the experimental cultures used in this study are at much higher cell densities than natural marine populations this project gives insight to the growth responses of a highly abundant photosynthetic organism, the cyanobacteria *Prochlorococcus marinus*.

Niche definitions of different *Prochlorococcus* strains involve a convolution of light level, temperature, and nutrient regimes (Moore et al., 1995). In addition to studying these environmental factors we added oxygen concentration as a potential factor driving *Prochlorococcus* niche partitioning, to pursue recent discoveries of *Prochlorococcus* niche

structuring by oxygen, as a major, differential influence upon growth rates of *Prochlorococcus marinus* strains.

The results from this project directly relate to the projected future community structure change in marine environments (Figure 2). *Prochlorococcus marinus* are one of the most abundant photosynthetic organisms on earth and play a fundamental role in regulating global carbon cycles, oxygen production, and marine food webs.

Conclusion and Future Research Opportunities

Previous studies have shown that clear niche-partitioning of *Prochlorococcus* strains are associated with environmental conditions including light intensity, temperature, and nutrient concentration, which has defined current ecotypes (Moore and Chisholm, 1999; Six et al., 2007; Yan et al., 2020). Thus, this study was undertaken to better understand the effect of light and oxygen regimes on the ability for *Prochlorococcus* cells to grow. It was found that *Prochlorococcus* MED4 has the highest cell density and chlorophyll exponential growth rates at 21% oxygen saturation under red (450nm) and blue (660nm) peaking at 180 µmol photons $m^{-2}s^{-1}$. Most strikingly, *Prochlorococcus* MIT9313 exhibits the most balanced growth at 0% oxygen saturation under red (660nm) light.

In this study the growth rate estimates were extracted and used to describe the biological responses of *Prochlorococcus* cells to varying environmental conditions. In contrast to growth rate Pmax values were not used in this study because the Pmax values were poorly constrained due to harvesting of many culture tubes before they reached Pmax. Furthermore, Pmax values in high density cultures in the lab are not comparable to naturally occurring densities in marine environments.

Future research on this project should include a time series analysis of diel cycling and most notably merge the growth parameter estimates from all runs across a common set of conditions. The barrier to these steps is imposed by the size of files, which could be overcome by implementing R analysis on a multi-core large memory Linux server or a statistical merger of logistic fit parameters from replicate tubes of the same conditions, by normalizing the intercepts to avoid offsets in starting cell suspension density.

To gain further insight as to how the physiology of *Prochlorococcus* cells respond to fluctuations in environmental conditions and oxygen concentrations a series of ROS analyses could be done. During this project we harvested cells from each run with intentions of completing immunoblotting analysis for RbcL crosslinks to research the cumulative effects of ROS on proteins within the cell. In addition to immunoblotting results, it would also be interesting to perform malondialdehyde assays to determine the cumulative effects of ROS on cellular lipids.

Bibliography

Andersson, I., Backlund, A., 2008. Structure and function of Rubisco. Plant Physiol. Biochem., Plant structural biology 46, 275–291. https://doi.org/10.1016/j.plaphy.2008.01.001

Bagby, S.C., Chisholm, S.W., 2015. Response of Prochlorococcus to varying CO 2 :O 2 ratios. ISME J. 9, 2232–2245. https://doi.org/10.1038/ismej.2015.36

Braakman, R., Follows, M.J., Chisholm, S.W., 2017. Metabolic evolution and the self-organization of ecosystems., Metabolic evolution and the self-organization of ecosystems. Proc. Natl. Acad. Sci. U. S. Am. Proc. Natl. Acad. Sci. U. S. Am. 114, 114, E3091, E3091–E3100. https://doi.org/10.1073/pnas.1619573114, 10.1073/pnas.1619573114

Campbell, L., Vaulot, D., 1993. Photosynthetic picoplankton community structure in the subtropical North Pacific Ocean near Hawaii (station ALOHA). Deep Sea Res. Part Oceanogr. Res. Pap. 40, 2043–2060. https://doi.org/10.1016/0967-0637(93)90044-4

Cooper, W.J., Saltzman, E.S., Zika, R.G., 1987. The contribution of rainwater to variability in surface ocean hydrogen peroxide. J. Geophys. Res. Oceans 92, 2970–2980. https://doi.org/10.1029/JC092iC03p02970

Dahl, T., RobertMiddenand, W., Hartman, P., 1987. Pure Singlet Oxygen Cytotoxicity for Bacteria. Photochem. Photobiol. 46, 345–352. https://doi.org/10.1111/j.1751-1097.1987.tb04779.x

Diaz, J.M., Plummer, S., 2018. Production of extracellular reactive oxygen species by phytoplankton: past and future directions. J. Plankton Res. 40, 655–666. https://doi.org/10.1093/plankt/fby039

Dowle, M., Srinivasan, A., 2019. data.table: Extension of “data.frame.”

Elzhov, T.V., Mullen, K.M., Spiess, A.-N., Bolker, B., 2016. minpacl.lm: R interface to the Levenberg-Marquardt Nonlinear Lest-Squares. Algorithm Found in MINPACK, Plus Support for Bounds.

Falkowski, P.G., 1994. The role of phytoplankton photosynthesis in global biogeochemical cycles. Photosynth. Res. 39, 235–258. https://doi.org/10.1007/BF00014586

Fernández-Pinos, M.-C., Casado, M., Caballero, G., Zinser, E.R., Dachs, J., Piña, B., 2015. Clade-Specific Quantitative Analysis of Photosynthetic Gene Expression in Prochlorococcus. PLOS ONE 10, e0133207. https://doi.org/10.1371/journal.pone.0133207

Flombaum, P., Gallegos, J.L., Gordillo, R.A., Rincón, J., Zabala, L.L., Jiao, N., Karl, D.M., Li, W.K.W., Lomas, M.W., Veneziano, D., Vera, C.S., Vrugt, J.A., Martiny, A.C., 2013. Present and future global distributions of the marine Cyanobacteria Prochlorococcus and Synechococcus. Proc. Natl. Acad. Sci. 110, 9824–9829. https://doi.org/10.1073/pnas.1307701110

Guerrero, S., 2014. 2. Dealing with Missing Data in R: Omit, Approx, or Spline Part 1 | Spencer Guerrero - University of Illinois at Urbana-Champaign. URL http://publish.illinois.edu/spencer-guerrero/2014/12/11/2-dealing-with-missing-data-in-r-omit-approx-or-spline-part-1/ (accessed 4.5.21).

Irigoien, X., Huisman, J., Harris, R.P., 2004. Global biodiversity patterns of marine phytoplankton and zooplankton. Nature 429, 863–867. https://doi.org/10.1038/nature02593

Ito, H., Tanaka, A., 2011. Evolution of a divinyl chlorophyll-based photosystem in Prochlorococcus. Proc. Natl. Acad. Sci. 108, 18014–18019. https://doi.org/10.1073/pnas.1107590108

Johnson, Z.I., Zinser, E.R., Coe, A., McNulty, N.P., Woodward, E.M.S., Chisholm, S.W., 2006. Niche Partitioning Among Prochlorococcus Ecotypes Along Ocean-Scale Environmental Gradients. Science 311, 1737–1740. https://doi.org/10.1126/science.1118052

Kieber, D., Peake, B., Scully, N., 2003. Reactive oxygen species in aquatic ecosystems. pp. 251–288. https://doi.org/10.1039/9781847552266-00251

Larkin, A.A., Blinebry, S.K., Howes, C., Lin, Y., Loftus, S.E., Schmaus, C.A., Zinser, E.R., Johnson, Z.I., 2016. Niche partitioning and biogeography of high light adapted Prochlorococcus across taxonomic ranks in the North Pacific. ISME J. 10, 1555–1567. https://doi.org/10.1038/ismej.2015.244

Latifi, A., Ruiz, M., Zhang, C.-C., 2009. Oxidative stress in cyanobacteria. FEMS Microbiol. Rev. 33, 258–278. https://doi.org/10.1111/j.1574-6976.2008.00134.x

Lavin, P., González, B., Santibáñez, J.F., Scanlan, D.J., Ulloa, O., 2010. Novel lineages of Prochlorococcus thrive within the oxygen minimum zone of the eastern tropical South Pacific. Environ. Microbiol. Rep. 2, 728–738. https://doi.org/10.1111/j.1758-2229.2010.00167.x

Mazard, S., Penesyan, A., Ostrowski, M., Paulsen, I.T., Egan, S., 2016. Tiny Microbes with a Big Impact: The Role of Cyanobacteria and Their Metabolites in Shaping Our Future. Mar. Drugs 14, 97. https://doi.org/10.3390/md14050097

Meunier, P.C., Colón-López, M.S., Sherman, L.A., 1998. Photosystem II Cyclic Heterogeneity and Photoactivation in the Diazotrophic, Unicellular CyanobacteriumCyanotheceSpecies ATCC 51142. Plant Physiol. 116, 1551–1562. https://doi.org/10.1104/pp.116.4.1551

Moore, L.R., Chisholm, S.W., 1999. Photophysiology of the marine cyanobacterium Prochlorococcus: Ecotypic differences among cultured isolates. Limnol. Oceanogr. 44, 628–638. https://doi.org/10.4319/lo.1999.44.3.0628

Moore, L.R., Goericke, R., Chisholm, S.W., 1995. Comparative physiology of Synechococcus and Prochlorococcus: influence of light and temperature on growth, pigments, fluorescence and absorptive properties. Mar. Ecol. Prog. Ser. 116, 259–275.

Morris, J.J., Johnson, Z.I., Szul, M.J., Keller, M., Zinser, E.R., 2011. Dependence of the Cyanobacterium Prochlorococcus on Hydrogen Peroxide Scavenging Microbes for Growth at the Ocean's Surface. PLOS ONE 6, e16805. https://doi.org/10.1371/journal.pone.0016805

Partensky, F., Hess, W.R., Vaulot, D., 1999. Prochlorococcus, a Marine Photosynthetic Prokaryote of Global Significance. Microbiol. Mol. Biol. Rev. 63, 106–127.

Perry, M.J., Talbot, M.C., Alberte, R.S., 1981. Photoadaption in marine phytoplankton: Response of the photosynthetic unit. Mar. Biol. 62, 91–101. https://doi.org/10.1007/BF00388170

Photo Systems Instruments, 2016. Software | Photobioreactors [WWW Document]. URL http://photo-bio-reactors.com/products/software/ (accessed 3.30.21).

Prabha, R., Singh, D.P., Gupta, S.K., Rai, A., 2014. Whole genome phylogeny of Prochlorococcus marinus group of cyanobacteria: genome alignment and overlapping gene approach. Interdiscip. Sci. Comput. Life Sci. 6, 149–157. https://doi.org/10.1007/s12539-013-0024-9

Price, D., Worsfold, P.J., C. Mantoura, R.F., 1992. Hydrogen peroxide in the marine environment: cycling and methods of analysis. TrAC Trends Anal. Chem. 11, 379–384. https://doi.org/10.1016/0165-9936(92)80028-5

Rabouille, S., Campbell, D.A., Masuda, T., Zavřel, T., Bernát, G., Polerecky, L., Halsey, K., Eichner, M., Kotabová, E., Stephan, S., Lukeš, M., Claquin, P., Bonomi-Barufi, J., Lombardi, A.T., Červený, J., Suggett, D.J., Giordano, M., Kromkamp, J.C., Prášil, O., 2021. Electron & Biomass Dynamics of Cyanothece Under Interacting Nitrogen & Carbon Limitations. Front. Microbiol. 12. https://doi.org/10.3389/fmicb.2021.617802

Rocap, G., Larimer, F.W., Lamerdin, J., Malfatti, S., Chain, P., Ahlgren, N.A., Arellano, A., Coleman, M., Hauser, L., Hess, W.R., Johnson, Z.I., Land, M., Lindell, D., Post, A.F., Regala, W., Shah, M., Shaw, S.L., Steglich, C., Sullivan, M.B., Ting, C.S., Tolonen, A., Webb, E.A., Zinser, E.R., Chisholm, S.W., 2003. Genome divergence in two Prochlorococcus ecotypes reflects oceanic niche differentiation. Nature 424, 1042–1047. https://doi.org/10.1038/nature01947

Scanlan, D.J., Ostrowski, M., Mazard, S., Dufresne, A., Garczarek, L., Hess, W.R., Post, A.F., Hagemann, M., Paulsen, I., Partensky, F., 2009. Ecological Genomics of Marine Picocyanobacteria. Microbiol. Mol. Biol. Rev. MMBR 73, 249–299. https://doi.org/10.1128/MMBR.00035-08

Schieber, M., Chandel, N.S., 2014. ROS Function in Redox Signaling and Oxidative Stress. Curr. Biol. 24, R453–R462. https://doi.org/10.1016/j.cub.2014.03.034

Six, C., Finkel, Z.V., Irwin, A.J., Campbell, D.A., 2007. Light Variability Illuminates Niche-Partitioning among Marine Picocyanobacteria. PLOS ONE 2, e1341. https://doi.org/10.1371/journal.pone.0001341

Strzepek, R.F., Boyd, P.W., Sunda, W.G., 2019. Photosynthetic adaptation to low iron, light, and temperature in Southern Ocean phytoplankton. Proc. Natl. Acad. Sci. 116, 4388–4393. https://doi.org/10.1073/pnas.1810886116

Thompson, C., Silva, G., Vieira, N., Edwards, R., Vicente, A., Thompson, F., 2013. Genomic Taxonomy of the Genus Prochlorococcus. Microb. Ecol. 66. https://doi.org/10.1007/s00248-013-0270-8

Wickham, H., 2017. tidyverse: Easily Install and Load the "Tidyverse."

Wickham, H., 2016. ggplot2: Elegant Graphics for Data Analysis. Springer-Verlag New York.

Yan, W., Feng, X., Zhang, W., Zhang, R., Jiao, N., 2020. Research advances on ecotype and sub-ecotype differentiation of Prochlorococcus and its environmental adaptability. Sci. China Earth Sci. 63, 1691–1700. https://doi.org/10.1007/s11430-020-9651-0

Zinser, E.R., Lindell, D., Johnson, Z.I., Futschik, M.E., Steglich, C., Coleman, M.L., Wright, M.A., Rector, T., Steen, R., McNulty, N., Thompson, L.R., Chisholm, S.W., 2009. Choreography of the Transcriptome, Photophysiology, and Cell Cycle of a Minimal Photoautotroph, Prochlorococcus. PLOS ONE 4, e5135. https://doi.org/10.1371/journal.pone.0005135

Appendices

MetaData Catalog: Google sheets link

Data is accessible via the following link:
https://docs.google.com/spreadsheets/d/1ZXpwR7Gfto-uRzVdXzMpQF4frbrvMLH_IyLqonFZRSw/edit#gid=0

Multi-Cultivator data: Dropbox link

Data is accessible via the following link:
https://www.dropbox.com/work/Phylis%20Campbell/Pico/MultiCultiData

Pro99 media preparation: Dropbox link

SOP is available via the following link:
https://www.dropbox.com/work/Phylis%20Campbell/CampbellLabProtocols/Culturing/Media?preview=Pro99+Medium.pdf

ASW preparation: Dropbox link

SOP is available via the following link:
https://www.dropbox.com/work/Phylis%20Campbell/CampbellLabProtocols/CampbellSOPs?preview=CampbellSOP4ASW.pdf

Rscript for data import: Dropbox link

Script is accessible via the following link:
https://www.dropbox.com/work/Phylis%20Campbell/Pico/R?preview=MultiDataImport.Rmd

Rscript for data tidying and logistic regression fits: Dropbox link

Script is accessible via the following link:
https://www.dropbox.com/work/Phylis%20Campbell/Pico/R?preview=MultiDataProcessLog.Rmd

Rscript for summary growth plots and balanced growth: Dropbox link

Script is accessible via the following link:
https://www.dropbox.com/work/Phylis%20Campbell/Pico/R?preview=MultiDataGrowthAssessLog.Rmd